Inner-ear sound pressures near the base of the cochlea in chinchilla: Further investigation

Michael E. Ravicz[a] and John J. Rosowski[b]
Eaton-Peabody Laboratory, Massachusetts Eye & Ear Infirmary, 243 Charles Street, Boston, Massachusetts 02114

(Received 31 August 2012; revised 4 January 2013; accepted 28 January 2013)

The middle-ear pressure gain $\mathbf{G_{MEP}}$, the ratio of sound pressure in the cochlear vestibule $\mathbf{P_V}$ to sound pressure at the tympanic membrane $\mathbf{P_{TM}}$, is a descriptor of middle-ear sound transfer and the cochlear input for a given stimulus in the ear canal. $\mathbf{G_{MEP}}$ and the cochlear partition differential pressure near the cochlear base $\Delta\mathbf{P_{CP}}$, which determines the stimulus for cochlear partition motion and has been linked to hearing ability, were computed from simultaneous measurements of $\mathbf{P_V}$, $\mathbf{P_{TM}}$, and the sound pressure in scala tympani near the round window $\mathbf{P_{ST}}$ in chinchilla. $\mathbf{G_{MEP}}$ magnitude was approximately 30 dB between 0.1 and 10 kHz and decreased sharply above 20 kHz, which is not consistent with an ideal transformer or a lossless transmission line. The $\mathbf{G_{MEP}}$ phase was consistent with a roughly 50-μs delay between $\mathbf{P_V}$ and $\mathbf{P_{TM}}$. $\mathbf{G_{MEP}}$ was little affected by the inner-ear modifications necessary to measure $\mathbf{P_{ST}}$. $\mathbf{G_{MEP}}$ is a good predictor of $\Delta\mathbf{P_{CP}}$ at low and moderate frequencies where $\mathbf{P_V} \gg \mathbf{P_{ST}}$ but overestimates $\Delta\mathbf{P_{CP}}$ above a few kilohertz where $\mathbf{P_V} \approx \mathbf{P_{ST}}$. The ratio of $\mathbf{P_{ST}}$ to $\mathbf{P_V}$ provides insight into the distribution of sound pressure within the cochlear scalae. © *2013 Acoustical Society of America*. [http://dx.doi.org/10.1121/1.4792139]

PACS number(s): 43.64.Ha, 43.64.Kc, 43.64.Tk [CHS] Pages: 2208–2223

I. INTRODUCTION

This paper is a continuation of our examination of sound power transmission through the external and middle ear (ME) to the cochlear partition (CP) (Ravicz and Rosowski, 2012b). In this paper we examine the ME pressure gain, defined as the transformation of ear canal (EC) sound pressure to sound pressure inside the oval window (OW), and the sound pressure difference across the CP near the base of the cochlea in chinchilla.

The middle-ear pressure gain $\mathbf{G_{MEP}}$, the ratio of sound pressure inside the OW $\mathbf{P_V}$ to EC sound pressure at the tympanic membrane (TM) $\mathbf{P_{TM}}$, is one descriptor of ME function (e.g., Shera and Zweig, 1992). $\mathbf{G_{MEP}}$ is a complex function of frequency f, with a magnitude $|\mathbf{G_{MEP}}|$ and a phase angle $\angle\mathbf{G_{MEP}}$, as are most sound pressures and transfer ratios described in this paper.[1] An advantage of using $\mathbf{G_{MEP}}$ over other ME descriptors is that sound pressures are scalar quantities rather than vectors and so are insensitive to the direction of measurement (in contrast to stapes velocity; e.g., Heiland *et al.*, 1999; de La Rochefoucauld *et al.*, 2008).

The differential sound pressure across the base of the CP $\Delta\mathbf{P_{CP}}$ is believed to be the driving force for basilar membrane motion, and several studies support this assumption (e.g., Dancer and Franke 1980; Lynch *et al.*, 1982; Voss *et al.*, 1996). Previous studies have estimated the drive to the basilar membrane from more peripheral measurements, e.g., stapes velocity or sound pressure near the OW. Recently we published preliminary results of a new investigation into the differential sound pressure across the CP near the base of the cochlea $\Delta\mathbf{P_{CP}}$ in chinchillas computed from measurements of $\mathbf{P_V}$ and in scala tympani (ST) near the round window (RW) $\mathbf{P_{ST}}$ in the same animals (normalized by sound pressure near the TM; Ravicz *et al.*, 2010). This paper continues that study with new data, refinements in technique, and a more complete discussion of the results.

This study also provides normative data for more definitive investigations of the hypothesized connection between $\Delta\mathbf{P_{CP}}$ and hearing. The "window-pressure difference" or "difference-mode" hypothesis of cochlear stimulation (e.g., von Békésy, 1947; Peake *et al.*, 1992; Voss *et al.*, 1996) suggests that the cochlear response (as measured by cochlear potentials) should be proportional to $\Delta\mathbf{P_{CP}}$. Normative results will aid in the understanding of the effect of different normal cochlear "third windows" (e.g., the cochlear and vestibular aqueduct) as well as various inner-ear pathologies on $\Delta\mathbf{P_{CP}}$ and hearing; e.g., inner-ear dehiscences (e.g., Songer and Rosowski, 2006), enlarged vestibular aqueduct, or RW atresia and fixation (see Merchant and Rosowski, 2008 for a review). These results will also help in the development of an animal model to evaluate the utility of direct RW stimulation (Lupo *et al.*, 2012).

Prior to 1998, nearly all studies of intracochlear sound pressure in animals used hydrophones connected to the cochlear scalae via probe tubes (Lynch *et al.*, 1982, in cat; Dancer and Franke, 1980, in guinea pig; Décory *et al.*, 1990, in cat, guinea pig, and chinchilla). In this study we use miniature fiber-optic pressure sensors developed by Olson (1998) with dimensions that allow placement of the entire transducer within the scalae.[2] These miniature sensors, which can be used in air or water, allow measurements close to the OW and RW and have been used to measure scalae sound pressures in live gerbils (e.g., Olson, 1998, 2001; Dong and

[a]Author to whom correspondence should be addressed. Electronic mail: mike_ravicz@meei.harvard.edu
[b]Also at Department of Otology and Laryngology, and Health Sciences and Technology, Harvard Medical School, Boston, MA 02115.

 0001-4966/2013/133(4)/2208/16/$30.00

Olson, 2006), live chinchillas (Slama *et al.*, 2010; Ravicz *et al.*, 2010), and human temporal bones (Nakajima *et al.*, 2009).

In this paper we present $\mathbf{G_{MEP}}$ and $\Delta\mathbf{P_{CP}}$ computed from measurements of $\mathbf{P_V}$, $\mathbf{P_{ST}}$, and sound pressure in the EC $\mathbf{P_{near\text{-}TM}}$ in seven individual chinchillas. [ME input admittance (Ravicz and Rosowski, 2012b) and stapes velocity (Ravicz *et al.*, 2011) were also measured in these same animals.] We also examine the effect of simple preparation-related ME and cochlear manipulations on $\mathbf{P_V}$, $\mathbf{P_{ST}}$, and $\Delta\mathbf{P_{CP}}$. The $\mathbf{G_{MEP}}$ and $\Delta\mathbf{P_{CP}}$ data presented here are part of the measurement set required for computation of power delivery to the cochlea and the CP by the ME.

II. METHODS

A. Preparation

These experiments were performed in accordance with guidelines published by the U.S. Public Health Service and were approved by the Massachusetts Eye & Ear Infirmary Institutional Animal Care and Use Committee. Seven chinchilla ears were used in this study and in the companion paper (Ravicz and Rosowski, 2012b). Animals remained alive throughout the experiment. The preparation and anesthesia[3] have been described in detail earlier (Ravicz and Rosowski, 2012b). The bony EC was greatly shortened in order to expose the TM to view, and a short brass tube (5 mm in diameter and 9 mm in length) was glued to the skull around the bony EC to allow the sound source (see Sec. II B) to be coupled repeatably to the ear. A stainless steel sleeve (0.8 mm inner diameter and 1.9 cm in length) was glued under the brass coupler to position the tip of a probe tube microphone to measure sound pressure $\mathbf{P_{near\text{-}TM}}$ within 1 to 1.5 mm of the umbo in the center of the TM. Thin sheets of bone posterior to the RW were removed to provide access to the bone covering the vestibule just posterior to the OW and to the surface of the cochlear capsule inferior and posterior to the RW.

A small hole was drilled through the vestibular wall posterior to the footplate with a fine pick, and a pressure sensor was introduced through the hole to measure sound pressure within the vestibule $\mathbf{P_V}$. The desired hole size was between 150 and 200 μm diameter, slightly larger than the sensor tip (145 μm diameter), but the resulting holes ranged from 170 to 340 μm diameter. The sensor was inserted to a depth of 150 to 500 μm into the vestibule. After $\mathbf{P_V}$ measurements, a similar small hole was made in the cochlear capsule approximately 1 mm inferior to the RW (near the apical extent of the "hook" region) with a 0.006 in. (150 μm) pivot drill to allow a second pressure sensor to be introduced into scala tympani for $\mathbf{P_{ST}}$ measurements. The hole provided a reasonably tight seal around the sensor tip, and the tip was placed approximately at the level of the inner cochlear wall. The location of the ST hole corresponded to a characteristic frequency (CF) of 12 to 18 kHz (Eldridge *et al.*, 1981; Müller *et al.*, 2010). Before the end of the experiment, the ossicular chain was interrupted by breaking the narrow shaft between the long process of the incus and the lenticular process.

B. Stimuli, responses, and equipment

Synthesized chirp and sinusoidal voltage stimuli were produced by a computer-controlled signal generator (33120 A, Hewlett-Packard, Palo Alto, CA). Stimulus levels were controlled by a programmable attenuator (PA-5, Tucker-Davis, Alachua, FL) and a reconstruction filter with programmable gain (3901, Krohn-Hite, Lake Mary, FL). A power amplifier (1001 A, Crest Audio, Meridian, MS) was used to drive (a) a low-impedance earphone (40-1377, Radio Shack, Fort Worth, TX) to generate sound in the EC or (b) a shaker for pressure sensor calibration. Three sound stimuli were used: A broadband chirp with uniform component magnitude from 49 Hz to 49 kHz, or one of two tone sequences: 98 Hz to 49 kHz at 6 pts/octave or, for better frequency resolution at high frequencies, 14 to 49 kHz at 12 pts/octave.[4]

Three responses were measured: (1) Sound pressure in air near the TM ($\mathbf{P_{near\text{-}TM}}$); and sound pressure in the perilymph (2) in the vestibule ($\mathbf{P_V}$) and (3) in scala tympani ($\mathbf{P_{ST}}$). $\mathbf{P_{near\text{-}TM}}$ was measured with a small microphone (FG23652, Knowles, Itasca, IL) attached to a thin probe tube. Scalae sound pressures were measured with fiber-optic pressure sensors (Olson, 1998) inserted into the scalae as described above. Responses were amplified if necessary (air sound pressure: Grass P5; scalae sound pressure: Custom differential amplifiers), digitized at 400 kHz by a data acquisition board (PCI6122 or PXI6122, National Instruments, Austin, TX), and saved on a computer. Up to four response channels could be saved at a time.

C. Calibrations

1. Ear canal microphone

The $\mathbf{P_{near\text{-}TM}}$ microphone, including the probe tube, was calibrated against 1/4 in. and 1/8 in. reference microphones as described previously (Ravicz *et al.*, 2010; Ravicz and Rosowski, 2012b). Repeated calibrations showed variations of generally less than 2 dB in magnitude and 0.01 cycle in phase.

2. Pressure sensors

Although a basic description of the calibration of the miniature pressure sensors has been presented previously (e.g., Olson, 1998; Ravicz *et al.*, 2010), several aspects of our experiments required us to expand the technique. We required greater precision in sensitivity, especially at high frequencies, and we needed to account for the temperature sensitivity of some sensors, as the temperature during calibration was lower than during use in live ears (body temperature). The expanded calibration technique is described below.

The pressure sensor calibration $\mathbf{S_P}(f)$ includes two components: (1) The frequency response of the sensor $\mathbf{S_f}(f)$, defined as the ratio of sensor output voltage $\mathbf{v_{sens}}(f)$ to sound pressure $\mathbf{P}(f)$ across frequency, normalized to 1 at a selected frequency f_0; and (2) the sensitivity S_0, defined as $|\mathbf{v_{sens}/P}|$ at f_0 (Ravicz *et al.*, 2010):

$$\text{Sensor calibration } \mathbf{S_P}(f) = S_0 \cdot \mathbf{S_f}(f), \tag{1a}$$

where

$$\text{frequency response } \mathbf{S_f}(f) = \frac{\mathbf{v_{sens}}(f)/\mathbf{P}(f)}{\mathbf{v_{sens}}(f_0)/\mathbf{P}(f_0)} \quad \text{and}$$

$$\text{sensitivity } S_0 = \left|\frac{\mathbf{v_{sens}}}{\mathbf{P}}\right|_{f_0}. \tag{1b}$$

For these sensors, the frequency response is nearly constant: The magnitude and phase of $\mathbf{S_f}(f)$ decrease smoothly and only slightly (by 2 to 10 dB and no more than 0.1 cycle) between 100 Hz and 50 kHz (see also Olson, 1998), and this frequency dependence is relatively constant during the active life of the sensor. In contrast, the sensitivity S_0 can be quite variable, and this variability affects all frequencies equally (Olson, 1998; Ravicz *et al.*, 2010). Additionally, in some sensors, the sensitivity S_0 varied with temperature, and limitations of our calibration setups (see below) precluded using a single measurement as a calibration across the entire frequency range. We therefore used a calibration constructed from several different types of measurements.

We used two stimulus methods: Air calibration, using a microphone; and water calibration, using a shaker, a small vial, and an accelerometer.

Air calibration provided a good estimate of the sensor frequency response above several kilohertz. For air calibration, the tip of the pressure sensor was positioned inside a closed calibration cavity to within 1 mm of a 1/8 in. reference microphone (see Ravicz *et al.*, 2007), and sensor and microphone outputs were measured in response to a tone sequence. This method had limited utility at lower frequencies (because a sound-tight seal could not be made without damaging the sensor; hence, we were not able to generate sufficiently high sound pressure to overcome the sensor noise floor) but was free of potential sources of error that affected water calibrations (see below) at frequencies above a few kilohertz.

Water calibration gave a more reliable estimate of the sensitivity *in vivo*, was well suited for measuring temperature effects, and was quicker and easier to perform during experiments but was subject to errors at low and high frequencies. For water calibrations, the sensor tip was submerged 1 mm deep into a small vial attached to a shaker head and accelerometer (4290, Brüel & Kjær, Denmark; see Nedzelnitsky, 1980). Acceleration of the vial in response to a tone stimulus generated a time-varying sound pressure in the vial [Schloss and Strasberg, 1962, Eq. (6)] expressed in the frequency domain

$$\mathbf{P}(f) = \rho_w\, h\, \ddot{\mathbf{X}}(f)\, \frac{\sin(\omega h/c)}{\cos(\omega h/c)\cos(\omega l/c)}, \tag{2a}$$

where ρ_w is the density of water, $\ddot{\mathbf{X}}(f)$ is the acceleration of the vial, h is the immersion depth of the sensor in the vial, l is the total depth of the water in the vial, c is the speed of sound in water, and $\omega = 2\pi f$. The fraction describes "wave effects," the relationship between the sound wavelength (in water) and the vial dimensions. In our setup, the wave effect fraction is negligible below about 20 kHz, and Eq. (2a) reduces to

$$\mathbf{P}(f) \approx \rho_w\, h\, \ddot{\mathbf{X}}(f)\ . \tag{2b}$$

The effect of temperature on probe sensitivity S_0 was assessed by heating the water and vial to chinchilla body temperature (37 °C) and measuring sensitivity repeatedly while the water cooled.[5] Temperature sensitivity was determined by averaging the response at each temperature over several low- and mid-frequency ranges where the signal-to-noise ratio was best.[6] During experiments, the vial and water were maintained at the highest temperature practical (usually 30 °C to 35 °C) to minimize the temperature difference between the calibration and body temperatures, and the sensors were calibrated before being inserted into the cochlear scala and immediately after being withdrawn.

Errors and uncertainty in water calibrations at low and high frequencies arose from several sources. Resonances in the sensor support excited by shaker and background vibrations contaminated calibrations at several low frequencies, especially near 300 to 400 and 900 to 1000 Hz. Limitations in shaker output at high frequencies caused a low signal-to-noise ratio, and bubbles in the vial and a shaker resonance near 50 kHz caused high-frequency calibration errors. Heating the vial increased bubble production, even when degassed distilled water was used. The effects of the vial dimensions [described by the fraction in Eq. (2a)] are 1 dB at 20 kHz and about 6 dB at 50 kHz.

We therefore constructed a calibration for each sensor from measurements described above and a simple model based on observations of many sensors (ours[7] and Elizabeth

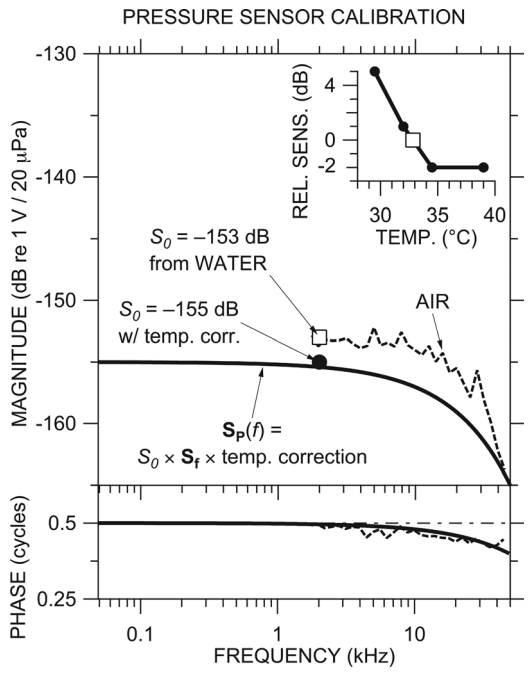

FIG. 1. Example of a pressure sensor calibration. The final calibration $\mathbf{S_P}(f)$ (thick black line) was constructed from the sensitivity S_0 of −153 dB (open square) from a water calibration in a vial evaluated at 2 kHz, high-frequency response $\mathbf{S_f}$ and phase accumulation modeled from air calibration (dashed line), and a correction for the temperature difference (inset) between calibration (at 33 °C; open square) and use (2 dB at 37 °C) (filled circle). Top: Magnitude; bottom: Phase.

Olson's, e.g., Olson, 1998) —see Fig. 1 for an example. For each set of scalae pressure measurements, we set the absolute sensitivity S_0 (open square in Fig. 1) equal to the mean of water calibration measurements at frequencies near $f_0 = 2$ kHz. In our example, $S_0 = -153$ dB re 1 V/20 μPa. The water calibration was made immediately after withdrawing the sensor from the inner ear (IE), in the belief (borne out by experience[8]) that the sensor was less likely to be damaged during withdrawal rather than upon insertion. S_0 was adjusted for the difference in temperature between the vial (33 °C in this example) and 37 °C, if necessary (−2 dB in our example; see Fig. 1 inset). Because all sensors showed a similar frequency response (similar to that shown in Fig. 2 of Olson, 1998), we modeled the frequency dependence of the sensitivity of each probe $\mathbf{S_f}$ as essentially flat, with a linear magnitude and phase roll-off with frequency determined by the air calibration (dashed curve in Fig. 1). The solid black line in Fig. 1 illustrates our best estimate of this sensor's frequency-dependent calibration $\mathbf{S_P}$ at body temperature, computed using Eq. (1) from $\mathbf{S_f}$ and the temperature-corrected S_0.

D. Noise floor, artifact, and frequency limits

Our measurements were limited at high frequencies by noise. Noise floor (microphones or pressure sensor) was determined practically by a measurement of the sensor output when no stimulus was present. In general, noise floors were computed from the measured spectra of the responses to tonal stimuli as the average of responses at nearby non-stimulus frequencies.[9] The high-frequency limit for $\mathbf{P_{TM}}$ was generally around 44 kHz, and for $\mathbf{P_V}$ and $\mathbf{P_{ST}}$, generally above 40 kHz. Data at frequencies where the responses were within 10 dB of the noise have been omitted.

An artifact, defined as spurious sensor response at a stimulus frequency, was determined for microphones by measuring microphone output with the probe tube plugged and was negligible. Because the artifact could not be measured directly for pressure sensors, we determined an upper bound on the artifact as the sensor output when the sensor was in the IE and the ossicular chain was interrupted [see Fig. 2(B)], a situation in which intracochlear sound pressures were expected to be reduced.

E. Course of experiment

Scalae and EC sound pressures were measured after making a hole into the cochlear vestibule and inserting a pressure sensor into it; after making a hole into scala tympani; after inserting a second sensor into the ST hole; and after interrupting the ossicular chain. In these conditions, ME input admittance (Ravicz and Rosowski, 2012b) and stapes velocity (Ravicz *et al.*, 2011) were also measured. The pressure sensors were calibrated before and after each of these measurements as described above. In most experiments, one

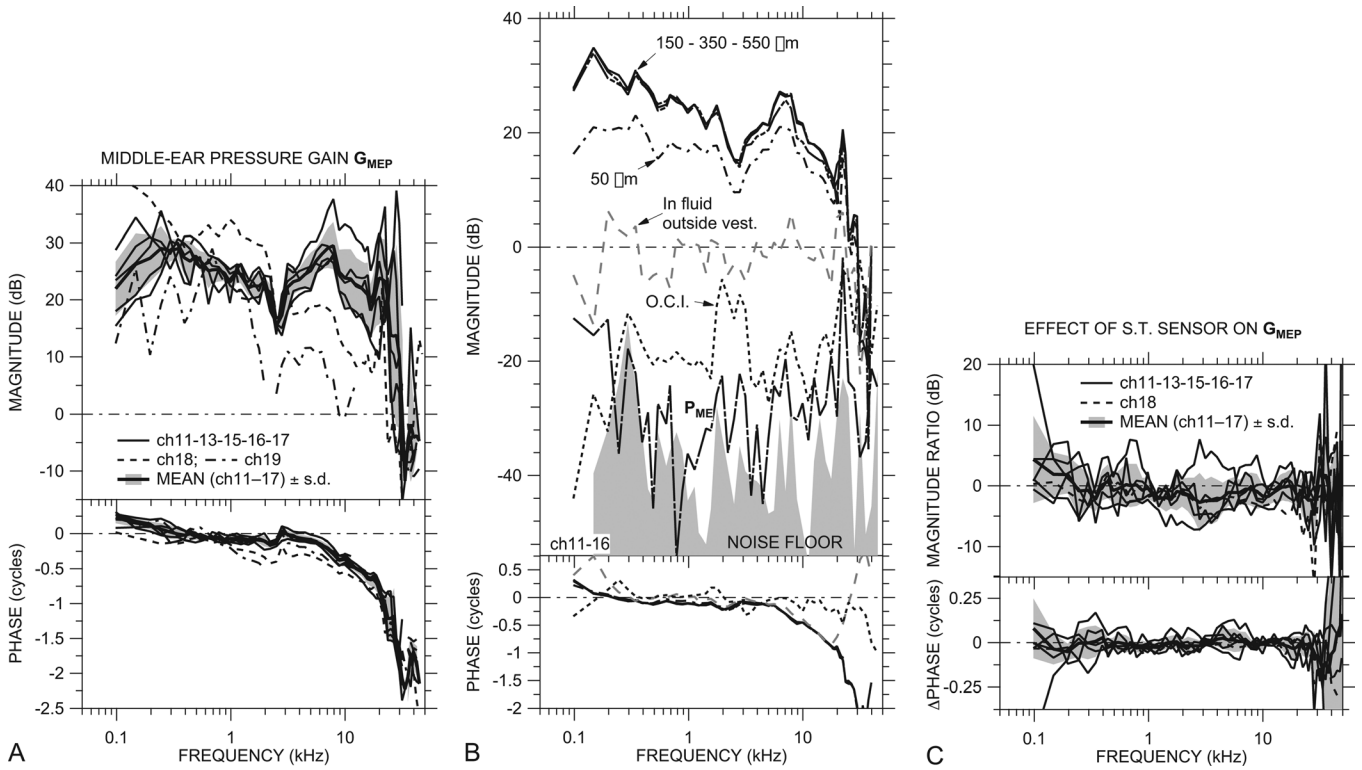

FIG. 2. (A) ME pressure gain $\mathbf{G_{MEP}}$ in dB in all ears with a sensor in the cochlear vestibule and intact scala tympani: ch18 (dashed line), ch19 (dotted-dashed line), and others (thin solid lines). Also shown is the mean $\mathbf{G_{MEP}}$ (thick solid line) ±1 s.d. (shaded area) of all ears except ch18 and ch19 (see the text). (B) $\mathbf{P_V}$ in an example ear (ch11) at different insertion depths (solid and dotted-dashed lines) and sound pressure in fluid outside the vestibule (dashed gray line); also, $\mathbf{P_V}$ with the ossicular chain interrupted (O.C.I.; dotted line), ME sound pressure (in air) $\mathbf{P_{ME}}$ (long-dashed-dotted line), and sensor noise floor for the O.C.I. measurement (shaded area) in another example ear (ch16). No phase data are shown for $\mathbf{P_{ME}}$ or the noise floor. All data are normalized by $\mathbf{P_{near\text{-}TM}}$. (C) Effect of opening ST and inserting a sensor on $\mathbf{G_{MEP}}$: Ratio of $\mathbf{G^T_{MEP}}$ with ST sensor in six ears to $\mathbf{G_{MEP}}$ with ST intact. Mean effect (thick solid line) ±1 s.d. (shading) of all ears except ch18 and ch19. All panels: Top: Magnitude; bottom: Phase.

or both pressure sensors failed at some point during the experiment and were replaced. Data shown below incorporate data from one or more sensors per ear and show no dependence on the sensor.

III. RESULTS

All quantities described in this section were measured with the ME widely opened and are normalized by sound pressure in the EC near the TM $\mathbf{P_{near\text{-}TM}}$.

A. Vestibule sound pressure P_V and ME pressure gain G_{MEP}

1. ST intact (sensor in vestibule)

ME pressure gain $\mathbf{G_{MEP}}$ with a sensor in the cochlear vestibule was computed from measurements of $\mathbf{P_V}$ and $\mathbf{P_{near\text{-}TM}}$ in seven ears by

$$\mathbf{G_{MEP}} = \mathbf{P_V}/\mathbf{P_{near\text{-}TM}}, \quad (3)$$

and is shown in Fig. 2(A). The curve for each ear is the logarithmic mean of 2 to 7 measurements; the standard deviation (s.d.) of these measurements was 1 to 2 dB. Several measurements with similar normalized results were taken in each ear at lower stimulus levels. Two ears (ch11, ch13) showed hints of a level dependence in $\mathbf{G_{MEP}}$ at low frequencies but no sign of response nonlinearity was seen in other ears. As described above, data at frequencies where $\mathbf{P_V}$ or $\mathbf{P_{near\text{-}TM}}$ may be contaminated by noise or artifact are omitted.

The magnitude of $\mathbf{G_{MEP}}$ was between 20 and 35 dB in nearly all ears (thin lines) between 150 Hz and 10 kHz, and $|\mathbf{G_{MEP}}|$ was somewhat lower at frequencies below a local maximum between 150 and 350 Hz. $\angle\mathbf{G_{MEP}}$ was near +0.25 cycles at the lowest frequencies in almost all ears and decreased to near 0 by 300 to 500 Hz. In all ears $\mathbf{G_{MEP}}$ showed a small magnitude dip and phase ripple around 2.5 kHz, presumably due to a resonance between the compliance of the air in the ME and the bulla hole (Rosowski *et al.*, 2006). At higher frequencies $|\mathbf{G_{MEP}}|$ increased again in almost all ears to a broad peak between 7 and 10 kHz, and $\angle\mathbf{G_{MEP}}$ steadily decreased. $\mathbf{G_{MEP}}$ magnitude and phase angle decreased gradually at frequencies above the broad peak, up to about 20 kHz. $\angle\mathbf{G_{MEP}}$ between 3 and 22 kHz is well fit by a delay of about 50 μs.

We observed another sharp peak in $|\mathbf{G_{MEP}}|$ between 21 and 28 kHz, and $\angle\mathbf{G_{MEP}}$ showed a 1/2-cycle decrease at the frequency of the $|\mathbf{G_{MEP}}|$ peak. Above the peak frequency, $|\mathbf{G_{MEP}}|$ decreased sharply to a value less than 0 dB. $\angle\mathbf{G_{MEP}}$ showed a 1/2-cycle increase between 32 and 35 kHz, then continued to decrease with frequency in some ears and was nearly constant in others. This $|\mathbf{G_{MEP}}|$ peak and 1/2-cycle $\angle\mathbf{G_{MEP}}$ step are discussed more in Sec. III D below.

$\mathbf{P_V}$ magnitude varied little with sensor insertion depth (up to 550 μm or so), as long as the sensor was inserted at least 150 to 200 μm into the vestibule, as shown for an example ear in Fig. 2(B). $|\mathbf{P_V}|$ decreased with shallower insertions.

$\mathbf{G_{MEP}}$ was similar among most ears except ch18 and ch19 (dashed and dotted-dashed lines, respectively). In these ears, $|\mathbf{G_{MEP}}|$ was lower by 10 to 15 dB above 2.5 kHz relative to measurements at 1 kHz, and $|\mathbf{G_{MEP}}|$ was lower in ear ch19 than in other ears across nearly the entire frequency range. Similarly, $\angle\mathbf{G_{MEP}}$ showed a greater phase lag in ears ch18 and ch19 than in the other ears at most frequencies. This lower $|\mathbf{G_{MEP}}|$, especially at high frequencies, would be expected if the ossicles were fractured or the ossicular joints were loosened. Stapes velocity was also lower in these ears (Ravicz *et al.*, 2011), consistent with ME damage,[10] and ME input admittance varied less upon interrupting the ossicular chain in these ears (Ravicz and Rosowski, 2012b).

Also shown in Fig. 2(A) is the mean (in the dB or logarithmic domain) of $\mathbf{G_{MEP}}$ in ears ch11, ch13, ch15, ch16, and ch17 (thick line) ±1 s.d. (shading). Data from ears ch18 and ch19 are omitted from the mean in this and all subsequent figures because of the suspected damage described above. The mean $\mathbf{G_{MEP}}$ captures the features of $\mathbf{G_{MEP}}$ in the five individual ears.

We checked the validity of $\mathbf{P_V}$ measurements by also measuring sound pressure with the sensor withdrawn from the vestibule but still in the fluid that accumulated in the OW niche, or in air in the open ME, also shown in Fig. 2(B). In this situation, the sensor measured the sum of (a) IE sound pressures radiated from the vestibule hole and RW and (b) ME sound pressure $\mathbf{P_{ME}}$ produced by the motion of the TM. The measured sound pressure magnitude in these situations was 20 to 60 dB lower than $|\mathbf{P_V}|$ when the sensor was in the vestibule ($\mathbf{P_{ME}}$ was virtually indistinguishable from the sensor noise floor), which suggests that our $\mathbf{P_V}$ measurements were influenced very little by sound pressures outside the cochlea.

As mentioned in Sec. II D above, $|\mathbf{P_V}|$ decreased substantially (20 to 50 dB) when the ossicular chain was interrupted ["OCI" in Fig. 2(B)]. In this case, the measured $\mathbf{P_V}$ is probably due mostly to sound conducted through the skull ("bone conduction"). The substantial reduction in phase accumulation supports this conclusion. As $\mathbf{P_V}$ in this case was the lowest vestibule pressure we could measure, it provides an upper bound to $\mathbf{P_V}$ stimulus artifact.

2. With a sensor in ST also

Sound pressure $\mathbf{P_V^T}$ was also measured in the vestibule in six of the seven ears (except ch19) with pressure sensors in both the vestibule and ST. Figure 2(C) shows the ratio of $\mathbf{G_{MEP}^T} = \mathbf{P_V^T}/\mathbf{P_{TM}}$ to $\mathbf{G_{MEP}}$ in each ear and the mean change of five ears (thick black line; shading indicates ±1 s.d.). Because the ST sensor had no effect on $\mathbf{P_{TM}}$, changes in $\mathbf{G_{MEP}}$ are directly attributable to changes in $\mathbf{P_V}$. In any ear, there were only small changes in $\mathbf{P_V}$ that were associated with the placement of the ST sensor, and the mean change showed virtually no effect. Placing the ST sensor caused a small (<2 dB) but statistically significant[11] reduction in $|\mathbf{G_{MEP}}|$ near 1.5 kHz but no other changes were significant. We use $\mathbf{P_V^T}$ measured simultaneously with $\mathbf{P_{ST}}$ in discussions of differential sound pressure below.

B. Normalized scala tympani sound pressure P_{STn}

1. Individuals and mean

Scala tympani sound pressure $\mathbf{P_{ST}}$ was measured in six of the seven ears (no $\mathbf{P_{ST}}$ measurements were made in ear

ch19), and $\mathbf{P_{STn}}$ ($\mathbf{P_{ST}}$ normalized by $\mathbf{P_{near\text{-}TM}}$) is shown in Fig. 3(A). Each curve is the logarithmic mean of two to five measurements, and several measurements with similar results were taken at lower stimulus levels. The normalized pressures showed no signs of stimulus level dependence. As above, data at frequencies where $\mathbf{P_{ST}}$ or $\mathbf{P_{near\text{-}TM}}$ may be contaminated by noise or artifact are omitted.

The magnitude of $\mathbf{P_{STn}}$ was similar in 5 of the 6 ears: In these 5 ears, $|\mathbf{P_{STn}}|$ was between 0 and +10 dB at the lowest frequencies measured, decreased below 0 dB between 150 and 900 Hz, and increased gradually with frequency (magnitude slope $\approx +1$: Dotted line) to 10 to 20 dB by about 5 kHz. All data points shown, even those near 400 Hz, are above noise and artifact (defined as for $\mathbf{G_{MEP}}$ above). $\angle\mathbf{P_{STn}}$ was generally near 0 between 500 Hz and 5 kHz and between −0.25 and 0 cycles at lower frequencies, although the variation among ears was higher at the lower frequencies. The magnitude dip and phase ripple in $\mathbf{P_{STn}}$ in all ears near 2.5 kHz is believed to be due to the bulla-hole resonance (see Sec. III A). $|\mathbf{P_{STn}}|$ was approximately constant between 5 and 20 kHz, and $\angle\mathbf{P_{STn}}$ accumulated steadily as frequency increased above about 5 kHz. The $\angle\mathbf{P_{STn}}$ slope with frequency between 3 and 22 kHz suggests a $\mathbf{P_{STn}}$ delay of about 50 μs, which is comparable to the $\mathbf{G_{MEP}}$ delay.

$\mathbf{P_{STn}}$ showed a sharp magnitude peak and 0.5-cycle phase change between 21 and 28 kHz as described for $\mathbf{G_{MEP}}$ above. $|\mathbf{P_{STn}}|$ decreased sharply at higher frequencies to <0 dB, and $\angle\mathbf{P_{STn}}$ decreased with frequency, similar to $\angle\mathbf{G_{MEP}}$ (Fig. 2) at high frequencies. In ear ch18, $|\mathbf{P_{STn}}|$ was higher than in other ears at the lowest frequencies and lower (≤0 dB) than in others at all other frequencies, and $\angle\mathbf{P_{STn}}$ showed more phase lag than the other ears at almost all frequencies.

In ear ch13, $\angle\mathbf{P_{STn}}$ was higher than in other ears below 800 Hz ($\mathbf{P_{STn}}$ was contaminated by an artifact below 350 Hz) but $\mathbf{P_{STn}}$ was similar to other ears at higher frequencies. In this ear there was a crack in the cochlear capsule caused by drilling the ST hole. This low-frequency behavior is similar to that seen previously in another ear with an otic capsule crack (Ravicz *et al.*, 2010).

We checked the validity of $\mathbf{P_{ST}}$ measurements by also measuring sensor output in some ears with the sensor withdrawn from ST: In the fluid that accumulated in the OW niche, or in air in the open ME (as described for $\mathbf{P_V}$ in Sec. III A 1). Sensor output in these circumstances was much lower than $|\mathbf{P_{ST}}|$, which suggests that our $\mathbf{P_{ST}}$ measurements were influenced very little by sound pressures outside the cochlea.

Also shown is the logarithmic mean of $\mathbf{P_{STn}}$ in ears ch11, ch13, ch15, ch16, and ch17 (thick line) ±1 s.d. (shading). Because the differences in $\mathbf{P_{STn}}$ between ear ch13 and the other ears occur only in $\angle\mathbf{P_{STn}}$ and only at low frequencies, we include it in the mean. The mean clearly captures the features of $\mathbf{P_{STn}}$ in individual ears.

2. Ratio of P_{ST} to P_V measured simultaneously

The ratio of simultaneous measurements of $\mathbf{P_{ST}}$ and $\mathbf{P_V^T}$ provides a useful view of the relationship between $\mathbf{P_{ST}}$ and $\mathbf{P_V^T}$. This ratio, defined as

$$\mathbf{rP_{ST}} = \mathbf{P_{ST}}/\mathbf{P_V^T}, \tag{4}$$

is shown in six ears in Fig. 3(B). $\mathbf{rP_{ST}}$ was similar among the 6 ears, except that $\mathbf{rP_{ST}}$ was about 10 dB lower in ear ch18 below 15 kHz than in the other ears. The mean $\mathbf{rP_{ST}}$ (thick line) ±1 s.d. (shading) was representative of $\mathbf{rP_{ST}}$ in the individual ears, and the ratio of mean $\mathbf{P_{ST}}$ to mean $\mathbf{P_V}$ was representative of the mean $\mathbf{rP_{ST}}$.

The $\mathbf{rP_{ST}}$ ratio showed different behavior in different frequency ranges. Below about 350 Hz $|\mathbf{rP_{ST}}|$ decreased as frequency increased, and $\angle\mathbf{rP_{ST}}$ was −0.25 cycles or less. There was a minimum in $|\mathbf{rP_{ST}}|$ of −30 dB or lower near

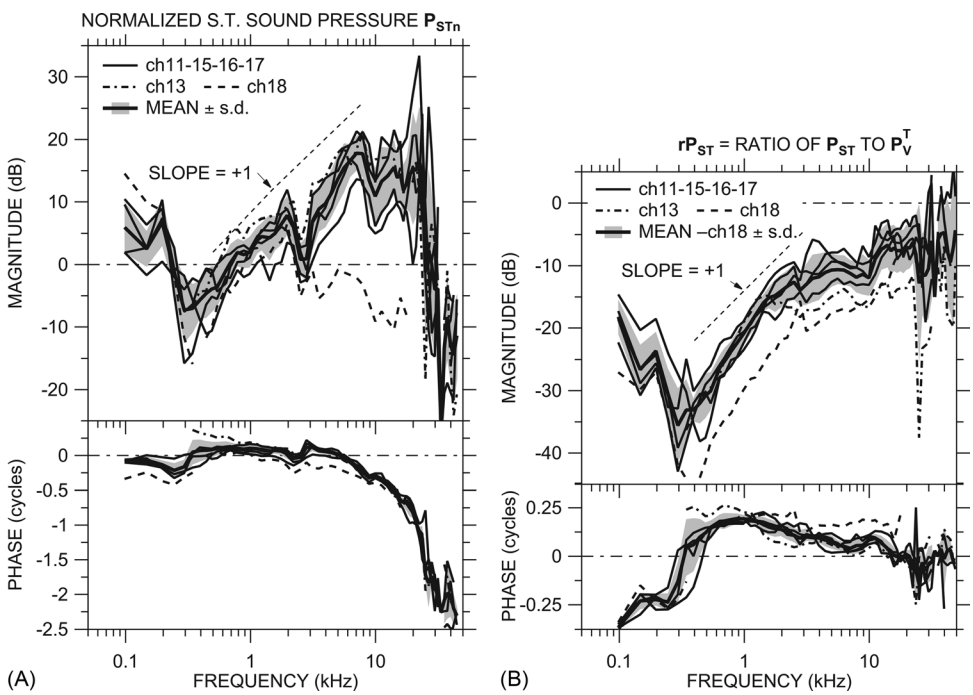

FIG. 3. (A) Scala tympani sound pressure $\mathbf{P_{STn}}$ (normalized by $\mathbf{P_{near\text{-}TM}}$) in dB in all ears: ch13 (dotted-dashed line), ch18 (dashed line), and others (thin solid lines). Also shown is the mean $\mathbf{P_{STn}}$ of all ears except ch18 (thick solid line) ±1 s.d. (shaded area). (B) Ratio of $\mathbf{P_{ST}}$ to $\mathbf{P_V^T} = \mathbf{rP_{ST}}$ in all ears measured. Line codes as in (A). Also shown is the mean $\mathbf{rP_{ST}}$ of all ears except ch18 (thick solid line) ±1 s.d. (shaded area). Both panels: Top: Magnitude; bottom: Phase; slope of +1 shown by dotted line.

350 Hz, and $\angle \mathbf{rP_{ST}}$ crossed 0 at that same frequency, which suggests that there is a resonance within the cochlea near 350 Hz (discussed further in Sec. IV D below).

Above the $|\mathbf{rP_{ST}}|$ minimum, $|\mathbf{rP_{ST}}|$ increased with frequency, with a slope of +1 (dotted line), to a plateau between −8 and −17 dB between about 3 and 10 kHz. $\angle \mathbf{rP_{ST}}$ was about +0.2 cycles in this frequency range ($\angle \mathbf{P_{ST}}$ led $\angle \mathbf{P_V}$) and gradually decreased, consistent with $\mathbf{P_V}$ and $\mathbf{P_{ST}}$ being controlled by different components (e.g., $\mathbf{P_V}$ by resistance and $\mathbf{P_{ST}}$ by mass). The slightly negative slope of $\angle \mathbf{rP_{ST}}$ with frequency is consistent with a small delay in $\mathbf{P_{ST}}$ relative to $\mathbf{P_V}$ (~5 μs) but is also consistent with a transition to the control of $\mathbf{P_V}$ and $\mathbf{P_{ST}}$ by similar acousto-mechanical components (e.g., both by mass).

In all ears, $|\mathbf{rP_{ST}}|$ abruptly increased to a higher plateau (−2 to −14 dB) above 10 kHz, and $\angle \mathbf{rP_{ST}}$ decreased to about 0 above 12 kHz. $\mathbf{rP_{ST}}$ remained constant at these values to the highest frequencies measured (45 kHz).

C. Differential pressure across the CP $\Delta \mathbf{P_{CP}}$

The driving force for input to the cochlear traveling wave is the differential sound pressure across the CP. We compute the normalized differential sound pressure $\Delta \mathbf{P_{CP}}$ near the cochlear base from simultaneous measurements of $\mathbf{P_V^T}$, $\mathbf{P_{ST}}$, and $\mathbf{P_{near\text{-}TM}}$ by

$$\Delta \mathbf{P_{CP}} = \frac{\mathbf{P_V^T} - \mathbf{P_{ST}}}{\mathbf{P_{near\text{-}TM}}} = \mathbf{G_{MEP}^T}(1 - \mathbf{rP_{ST}}). \quad (5)$$

$\Delta \mathbf{P_{CP}}$ computed in each of the six ears by Eq. (4) [Fig. 4(A)] was generally quite similar to $\mathbf{G_{MEP}}$ measured in those ears without the ST hole (Fig. 2) or with the ST sensor ($\mathbf{G_{MEP}^T}$). The mean $\Delta \mathbf{P_{CP}}$ is representative of $\Delta \mathbf{P_{CP}}$ in most individual ears, although the s.d. of the mean (shading) is larger than the s.d. of $\mathbf{P_{STn}}$ or $\mathbf{G_{MEP}}$. The change in $\angle \Delta \mathbf{P_{CP}}$ with frequency is consistent with a delay of about 50 μs.

The ratio of $\Delta \mathbf{P_{CP}}$ to $\mathbf{G_{MEP}^T}$ measured simultaneously [Fig. 4(B)] emphasizes the similarity between $\Delta \mathbf{P_{CP}}$ and $\mathbf{G_{MEP}^T}$ at low frequencies and highlights the differences at high frequencies. Below 3 kHz $\Delta \mathbf{P_{CP}} \approx \mathbf{G_{MEP}^T}$ because $|\mathbf{P_{ST}}| \ll |\mathbf{P_V^T}|$ [$|\mathbf{rP_{ST}}| \ll 1$; see Fig. 3(B)]. At higher frequencies $|\Delta \mathbf{P_{CP}}| < |\mathbf{G_{MEP}^T}|$ by 5 to 10 dB because the magnitude and phase of $\mathbf{P_{ST}}$ and $\mathbf{P_V^T}$ are similar [$|\mathbf{rP_{ST}}|$ is about −10 dB and $\angle \mathbf{rP_{ST}} \approx 0$; see Fig. 3(B)]. $\mathbf{G_{MEP}^T}$ [and $\mathbf{G_{MEP}}$, because $\mathbf{G_{MEP}^T} \approx \mathbf{G_{MEP}}$; see Fig. 2(C)] is a good predictor of $\Delta \mathbf{P_{CP}}$ at low frequencies but overestimates $|\Delta \mathbf{P_{CP}}|$ at frequencies above a few kilohertz.

D. High-frequency correction to $\mathbf{P_{TM}}$, $\mathbf{G_{MEP}}$, and $\Delta \mathbf{P_{CP}}$

A question of recent interest concerns the presence or absence of some high-frequency limit on ME function. In this section we use an EC model developed earlier (Ravicz and Rosowski, 2012b, Fig. 4) to investigate limitations in our measurements of sound pressure near the TM on $\mathbf{G_{MEP}}$ and $\Delta \mathbf{P_{CP}}$ at higher frequencies.

1. P_{TM} correction from the EC model

In a previous paper we presented a simple uniform-tube acoustical model of the chinchilla EC that successfully predicted the ratio of sound pressures measured at two points in the EC, at the $\mathbf{P_{near\text{-}TM}}$ measurement location near the TM and near the entrance to the sound coupler (see Ravicz and Rosowski, 2012b, Fig. 1). This model suggests that sound pressure at the near-TM location $\mathbf{P_{near\text{-}TM}}$ (1 to 1.5 mm from the TM) can differ substantially from the sound pressure at the TM $\mathbf{P_{TM}}$ at frequencies above 16 kHz. Figure 5(A) shows the model prediction of $\hat{\mathbf{P}}_{\mathbf{near-TM}}$ (dashed line) from Ravicz and Rosowski (2012b, Fig. 3) as well as the predicted sound pressure approximately at the TM location

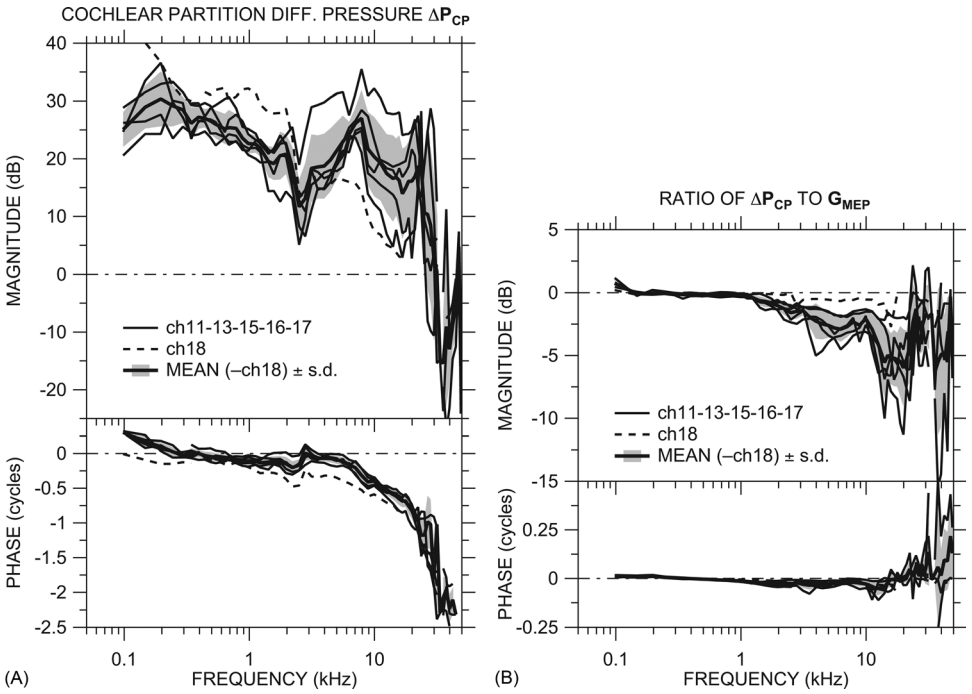

FIG. 4. (A) Differential sound pressure across the CP at the base $\Delta \mathbf{P_{CP}}$ in dB in all ears: ch18 (dashed line) and others (thin solid lines). Also shown is the mean $\Delta \mathbf{P_{CP}}$ (thick solid line) of all ears except ch18 ± 1 s.d. (shaded area). (B) Ratio of $\Delta \mathbf{P_{CP}}$ to $\mathbf{G_{MEP}}$ in all ears: ch18 (dashed line), others (thin solid lines), and mean (omitting ch18) ±1 s.d. (thick solid line and shaded area). All panels: Top: Magnitude; bottom: Phase.

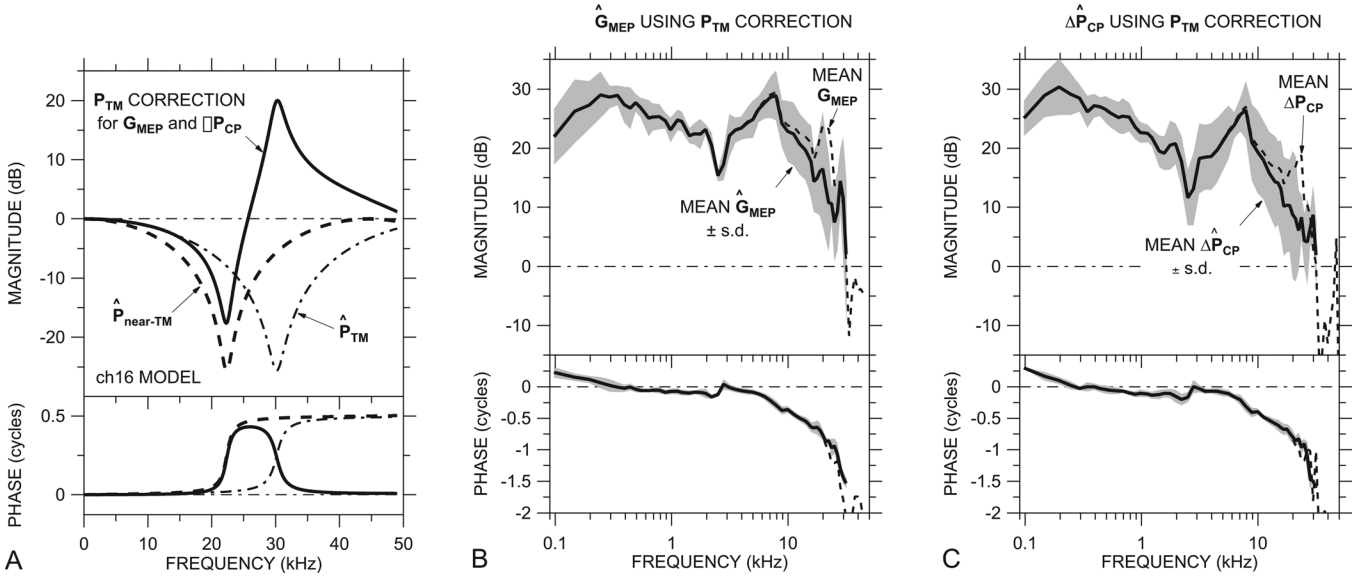

FIG. 5. (A) Correction factor $\mathbf{c\hat{P}_{TM}}$ (solid line) to estimate sound pressure at the TM $\mathbf{P_{TM}}$ from measured $\mathbf{P_{near\text{-}TM}}$ in an example ear (ch16), computed as the inverse of the ratio of $\mathbf{\hat{P}_{TM}}$ (dotted-dashed line) to $\mathbf{\hat{P}_{near\text{-}TM}}$ (dashed line; both normalized by sound pressure at the EC termination) in an ear-canal model. (B) Predicted mean $\mathbf{\hat{G}_{MEP}}$ ±1 s.d. (thick line and shading) and (C) predicted mean $\mathbf{\Delta\hat{P}_{CP}}$ ± 1 s.d. (thick line and shading) computed from $\mathbf{P_V}$, $\mathbf{P_{ST}}$, and $\mathbf{P_{near\text{-}TM}}$ using a $\mathbf{c\hat{P}_{TM}}$ correction for each ear as in (A). The uncorrected $\mathbf{G_{MEP}}$ (Fig. 2) and $\mathbf{\Delta P_{CP}}$ (Fig. 4) are shown by dashed lines. All panels: Top: Magnitude; bottom: Phase.

$\mathbf{\hat{P}_{TM}}$ (dotted-dashed line), 1 mm closer to the model EC termination in an example ear (ch16).[12] [In Fig. 5(A), both $\mathbf{\hat{P}_{near\text{-}TM}}$ and $\mathbf{\hat{P}_{TM}}$ are normalized by the sound pressure at the termination of the model EC.] A comparison of these curves suggests that $|\mathbf{P_{near\text{-}TM}}|$ underestimates sound pressure 1 mm closer to the TM by more than 15 dB around 22 kHz and overestimates it by more than 15 dB around 30 kHz.

Figure 5(A) also shows a correction factor $\mathbf{c\hat{P}_{TM}}$ for this ear, computed as $\mathbf{c\hat{P}_{TM}} = (\mathbf{\hat{P}_{TM}}/\mathbf{\hat{P}_{near-TM}})^{-1}$ (thick solid line), that could be applied to $\mathbf{P_{near\text{-}TM}}$ to compute a more accurate estimate of $\mathbf{P_{TM}}$ in ear ch16. Using the model, we developed a $\mathbf{c\hat{P}_{TM}}$ correction for each ear from appropriate EC parameters (see Ravicz and Rosowski, 2012b, Table I) and computed improved estimates of $\mathbf{G_{MEP}}$ and $\mathbf{\Delta P_{CP}}$ for each ear by

$$\mathbf{\hat{G}_{MEP}} = \mathbf{G_{MEP}} \cdot \mathbf{c\hat{P}_{TM}} \tag{6a}$$

and

$$\mathbf{\Delta\hat{P}_{CP}} = \mathbf{\Delta P_{CP}} \cdot \mathbf{c\hat{P}_{TM}}. \tag{6b}$$

The frequency of the peak in $|\mathbf{c\hat{P}_{TM}}|$ (27 to 42 kHz, depending on the ear) depends on the distance from the near-TM measurement location to the TM. We have made the conservative assumption that this distance was 1 mm; if the distance were actually closer to 1.5 mm, the peak in $|\mathbf{c\hat{P}_{TM}}|$ for ear ch16 (our example) would be closer to 36 kHz, and estimates of $\mathbf{\hat{P}_{TM}}$ near 30 kHz would be in error. Because of errors due to this uncertainty in the distance between the probe tube tip and the TM, we omit data above the frequency where the variation in $\mathbf{c\hat{P}_{TM}}$ due to the distance uncertainty exceeds the s.d. of the mean $\mathbf{G_{MEP}}$ (roughly a factor of 2): 24 to 34 kHz, depending on the ear.

2. G_{MEP} and ΔP_{CP} with P_{TM} correction

The predicted mean $\mathbf{\hat{G}_{MEP}}$ and $\mathbf{\Delta\hat{P}_{CP}}$ ±1 s.d. are shown in Figs. 5(B) and 5(C), respectively (solid line and shaded area in each panel). Also shown are the mean uncorrected $\mathbf{G_{MEP}}$ and $\mathbf{\Delta P_{CP}}$ (dashed lines) from Figs. 2(A) and 4(A), respectively. The effects of the $\mathbf{c\hat{P}_{TM}}$ correction are to remove the peak in $|\mathbf{G_{MEP}}|$ and $|\mathbf{\Delta P_{CP}}|$ between 21 and 28 kHz and to increase $\angle\mathbf{G_{MEP}}$ and $\angle\mathbf{\Delta P_{CP}}$ between about 25 kHz and the highest frequency (31 kHz). Note that the $\mathbf{rP_{ST}}$ data of Fig. 3(B) are unaffected by uncertainties in EC sound pressure, as $\mathbf{rP_{ST}}$ is a ratio of scalae pressures and does not include EC sound pressure, so no $\mathbf{c\hat{P}_{TM}}$ correction is necessary.

These predictions of $\mathbf{\hat{G}_{MEP}}$ and $\mathbf{\Delta\hat{P}_{CP}}$ represent our best estimates of $\mathbf{G_{MEP}}$ and $\mathbf{\Delta P_{CP}}$ at high frequencies. Application of the $\mathbf{c\hat{P}_{TM}}$ correction removed a peak in $\mathbf{G_{MEP}}$ and $\mathbf{\Delta P_{CP}}$ and reduced the frequency where the magnitude begins to roll off with frequency. We will use the notation $\mathbf{G_{MEP}}$ and $\mathbf{\Delta P_{CP}}$ for $\mathbf{\hat{G}_{MEP}}$ and $\mathbf{\Delta\hat{P}_{CP}}$ in the following sections.

IV. DISCUSSION

We have presented the results of measurements of sound pressure in the EC, vestibule, and ST in individual chinchillas and computed the CP differential pressure $\mathbf{\Delta P_{CP}}$. In this section we (a) examine the assumption that these sound pressures are primarily compressional or "fast-wave" pressures little influenced by basilar membrane motion (e.g., Olson, 1998; Dong and Olson, 2008). We (b) examine the effects of experimental conditions on our measurements and computed values and (c) compare our results to those from previous studies. We (d) discuss the implications of our $\mathbf{rP_{ST}}$ results and $\mathbf{rP_{ST}}$ computed from other studies on cochlear

mechanics and (e) examine the advantages and limitations of the chinchilla model for further studies of the effects of cochlear pathologies and manipulations on hearing.

A. Validity of compressional-wave assumption

The intracochlear sound pressures we measured are the sum of a compressional cochlear pressure wave that propagates virtually instantaneously throughout the cochlea and a traveling pressure wave associated with motion of the CP (Dong and Olson, 2008).[13] We assumed in Sec. III that our measured $\mathbf{P_V}$ and $\mathbf{P_{ST}}$ were due primarily to the compressional wave. $\mathbf{P_V}$ was measured in the vestibule just posterior to the OW. Our $\mathbf{P_V}$ and the SV pressure measured in gerbil at locations on the cochlear side of the OW showed no signs of the frequency-dependent nonlinearities or rapid phase accumulation associated with traveling-wave effects (Olson, 1998; Dong and Olson, 2008), so we believe that our measured $\mathbf{P_V}$ is dominated by the compressional wave and that the contribution of the traveling wave is negligible.

The likelihood that our $\mathbf{P_{ST}}$ measurements include contributions from the cochlear traveling wave varies in different frequency ranges, as the distance that the traveling wave penetrates ST at a given location varies with the ratio of stimulus frequency to the CF at that location (Olson, 2001; Yoon *et al.*, 2006). As discussed above, signs of traveling wave contributions include $\angle\mathbf{P_{ST}}$ accumulation, $|\mathbf{P_{ST}}|$ level dependence, and $|\mathbf{P_{ST}}|$ notches in the half-octave below CF (Cooper and Rhode, 1996; Olson, 1998, 2001).

At frequencies well below CF at our $\mathbf{P_{ST}}$ measurement location, $\mathbf{P_{ST}}$ represents the compressional wave, as $\mathbf{P_{ST}}$ was measured relatively far from the CP, and the traveling wave should be detectable only very close to the CP (Olson, 2001; Yoon *et al.*, 2006). In this "long-wavelength" regime, the relationship between $\mathbf{P_V}$ and $\mathbf{P_{ST}}$ can be described by lumped model elements (Ravicz *et al.*, 2010). Figure 3(B) shows that the phase angle difference between $\mathbf{P_{ST}}$ and $\mathbf{P_V}$ ($\angle\mathbf{rP_{ST}}$) was always within ± 0.25 cycles (except below at the lowest frequencies) and that $\angle\mathbf{rP_{ST}}$ tended not to accumulate with frequency, consistent with a lumped-element model.

Near CF ($\sim$12 kHz), traveling wave effects extend further into ST from the CP (Olson, 2001; Yoon *et al.*, 2006).[14] We saw little evidence of level dependence in $\mathbf{P_{ST}}$ but the abrupt increase in $|\mathbf{P_{ST}}|$ and decrease in $\angle\mathbf{P_{ST}}$ near 12 kHz might be due to a contribution from the traveling wave. These are discussed more in Sec. IV D below.

At frequencies above CF, the traveling wave is absent, and our $\mathbf{P_{ST}}$ represents the compressional wave (perhaps including a contribution from a fast evanescent wave invoked to explain observations of non-zero basilar membrane motion above CF; de La Rochefoucauld and Olson, 2007). $|\mathbf{rP_{ST}}|$ was about -6 dB in all ears, similar to its value near CF (see above), and $\mathbf{P_V}$ and $\mathbf{P_{ST}}$ were in phase ($\angle\mathbf{rP_{ST}} \approx 0$), although the variability of both $|\mathbf{rP_{ST}}|$ and $\angle\mathbf{rP_{ST}}$ was higher, perhaps due to noise. The result that $|\mathbf{rP_{ST}}|$ was constant and $\angle\mathbf{rP_{ST}} \approx 0$ at these highest frequencies is consistent with $\mathbf{P_V}$ and $\mathbf{P_{ST}}$ determined by the compressional wave.

It should be noted that the condition that the compressional wave propagates virtually *instantaneously* throughout the cochlea does not imply that the sound pressure is *uniform* throughout the cochlea. Because the RW impedance is much lower than the cochlear input impedance at moderate and high frequencies (compare Nedzelnitsky, 1980 and Lynch *et al.*, 1982 in cat; Slama *et al.*, 2010 and Ravicz *et al.*, 2010 in chinchilla), the RW acts as a zero-pressure boundary condition, and intracochlear pressure must vary continuously from $\mathbf{P_V}$ at the OW to approximately zero at the RW. The observation that $|\mathbf{P_{ST}}| \ll |\mathbf{P_V}|$ below about 2 kHz supports this view. This pressure gradient has been predicted to vary along the CP in a non-uniform and frequency-dependent fashion, as it is affected by the local CP impedance (e.g., Peterson and Bogert, 1950; Lighthill, 1981) as well as the acoustic impedances of the enclosed scalae (Puria and Allen, 1991) and the helicotrema (Dallos, 1970; Lynch *et al.*, 1982). We will discuss the implications of variations in $\mathbf{rP_{ST}}$ in Sec. IV D below.

B. Effect of experimental conditions on measured quantities

For these experiments it was necessary to make two large holes in the auditory bulla for access to the stapes, OW and RW, and stapedius muscles (see Sec. II A). The measurement of $\mathbf{P_V}$ required that a hole be made into the cochlear vestibule, and the measurement of $\mathbf{P_{ST}}$ required that an additional hole be made into ST.

1. Estimated effect of opening the ME

Measuring the effect of opening the ME on $\mathbf{P_V}$ was difficult, as we needed to open the ME to introduce the $\mathbf{P_V}$ sensor into the IE.[15] It has been shown (e.g., Zwislocki, 1962; Ravicz *et al.*, 1992; Huang *et al.*, 1997) that the impedance related to the compression and rarefaction of the air in the ME cavities (air spaces) can be considered to act "in series" with the impedance of the TM, ossicles, and cochlea; consequently, variations in ME cavity impedance, for instance, by opening holes in the bulla, have no effect on the cochlear input impedance (the ratio of $\mathbf{P_V}$ to stapes velocity). This independence of the cochlear input impedance means that the effect of opening the ME on $\mathbf{P_V}$ is the same as the effect on stapes velocity.

Ruggero *et al.* (1990) used umbo velocity measurements and previous studies of cochlear microphonic to infer that the effect of opening the ME on stapes velocity was the same as the effect on umbo velocity, which they showed was significant only at low frequencies (less than a factor of 2 above 300 Hz; Ruggero *et al.*, 1990, Figs. 5 and 6). It has been shown that the resonant frequency between the compliance of the air within the ME cavities and the mass of the air in the bulla holes varies with hole size (Rosowski *et al.*, 2006). Above the resonant frequency, the effects of opening the hole are insignificant. Although we have no information on the size of the bulla hole or hole-cavity resonant frequency in the Ruggero *et al.* (1990) experiments, we assume that the resonant frequency for effects on stapes velocity and ME admittance is the same for a given hole size. The bulla hole size used in this and previous studies caused an increase in ME input admittance magnitude and a -0.25 cycle phase

shift below 1 kHz (Ravicz and Rosowski, 2012b; Rosowski *et al.*, 2006), and we assume that the effect on stapes velocity and therefore $\mathbf{P_V}$ was similar.

Because $\mathbf{P_V}$ is the principal driving force for $\mathbf{P_{ST}}$ (Nedzelnitsky, 1980), the effect of opening the ME on $\mathbf{P_{ST}}$ is expected to be similar to the effect on $\mathbf{P_V}$. $\mathbf{P_{ST}}$ might also be affected by sound pressure outside the RW (Peake *et al.*, 1992) but our measurements of ME sound pressure outside the OW [Fig. 2(B)] and RW are at least 40 dB lower than $\mathbf{P_V}$, and measurements of ME sound pressure with an intact or open ME (personal communication from D. C. Chhan, 2012) demonstrate that the effects of ME sound pressures outside the OW and RW are negligible.

We did observe a magnitude notch and phase ripple in $\mathbf{G_{MEP}}$ and $\mathbf{P_{STn}}$ near 2.5 kHz, the frequency of a resonance observed in the ME input admittance (Ravicz and Rosowski, 2012b) between the acoustic mass of the bulla hole and the acoustic compliance of the air in the ME.

2. Effect of vestibule hole and sensor on P_V

Because our technique for measuring $\mathbf{P_V}$ required making a hole into the vestibule, we were unable to determine the effect of the IE hole and vestibule sensor on $\mathbf{P_V}$, and the narrow OW niche precluded sealing the hole around the sensor.[15] Previous measurements in cat (Lynch *et al.*, 1982) indicate that the hole will decrease the cochlear input impedance and therefore $\mathbf{P_V}$ at low frequencies. The theoretical impedance of the hole increases with frequency (e.g., Beranek, 1986; Slama *et al.*, 2010), so its effect on the cochlear input impedance and therefore $\mathbf{P_V}$ should decrease as frequency increases. Since the impedance of the hole depends inversely on a high power of its radius (or, in this case, on the distance between the edge of the hole and the sensor; e.g., Backus, 1975; Beranek, 1986), larger holes were expected to have larger effects. For this reason, we tried to make the hole as close to the sensor size as possible but the resulting hole was generally two times the diameter of the sensor or more.

Several observations suggest that the effect of the vestibule hole is most significant at low frequencies and less important at higher frequencies: (a) Withdrawing the sensor from the vestibule (leaving the hole open) caused a 5 to 9 dB reduction in $|\mathbf{P_{STn}}|$ below 1 kHz but very little change at higher frequencies. (b) Slama *et al.* [2010, Fig. 3(C)] were able to increase low-frequency $\mathbf{G_{MEP}}$ slightly in one ear by sealing around the sensor but saw no effect above a few hundred hertz. (c) Ravicz *et al.* (2010) observed that in ears where the bone near the OW cracked (equivalent to a large vestibule hole), $\mathbf{G_{MEP}}$ was substantially lower at frequencies below 1 kHz than in other ears where the bone was not cracked but very similar at higher frequencies. (d) Opening the IE and inserting the vestibule sensor caused an increase in stapes velocity that was largest (a factor of $3 \approx 10$ dB) below 500 Hz (Ravicz *et al.*, 2011). The size of the effect of the hole on low-frequency $\mathbf{G_{MEP}}$ is not known, but a mathematical analysis suggests that the hole reduces $|\mathbf{G_{MEP}}|$ by 15 dB at 100 Hz and has a negligible effect above 250 Hz (Ravicz and Rosowski, 2012a).

The pressure sensor itself could affect IE pressure measurements if its impedance were comparable to or lower than the cochlear input impedance (e.g., Olson, 1998). The impedance of the sensor's enclosed air volume (<1 nl), a conservative estimate of sensor impedance, is at least a factor of 10 larger than the cochlear input impedance (e.g., Slama *et al.*, 2010) at frequencies below 30 kHz; therefore, the effect of the sensor on the measured IE pressures is negligible.

We did not find a strong correlation between the size of the vestibule hole and aspects of low-frequency $|\mathbf{G_{MEP}}|$. There was a weak correlation between the hole area and the frequency of the low-frequency $|\mathbf{G_{MEP}}|$ peak but we saw no correlation between the hole area and $\mathbf{G_{MEP}}$ magnitude.

During the experiment, fluid frequently collected in the OW niche, which could conceivably have added an additional mass load on the ossicular chain and reduced $\mathbf{P_V}$ (and therefore $\mathbf{P_{ST}}$) at high frequencies. The effect of OW fluid contributes to the variability of $\mathbf{G_{MEP}}$ (and therefore $\mathbf{P_{STn}}$) in individual ears but should not affect $\mathbf{rP_{ST}}$. The RW remained above the fluid level and dry, so $\mathbf{P_{ST}}$ should not have been affected directly by OW fluid.

3. Effect of ST hole and sensor on P_V and P_{ST}

Opening ST and inserting another sensor to measure $\mathbf{P_{ST}}$ had only a small effect on $\mathbf{P_V}$, as shown in Fig. 2(C) above. This result is reasonable: (a) The hole for the ST sensor was generally a closer fit to the sensor and longer than the vestibule hole (the bone of the otic capsule was thicker than the vestibular wall), which would make its impedance very high and make the hole appear acoustically closed at the frequencies measured; and (b) most effects of the hole are probably masked by the effect of the low-impedance RW (see Lynch *et al.*, 1982, in cat).

It was not possible to measure the effect of the ST sensor on $\mathbf{P_{ST}}$ for the reason described above for $\mathbf{P_V}$. The observation that $|\mathbf{P_{ST}}| > |\mathbf{P_{near\text{-}TM}}|$ at very low frequencies [$|\mathbf{P_{STn}}| > 0$ dB below 250 Hz; Fig. 3(A)], where the effect of the ST hole should be maximal (by the reasoning in Sec. IV B 2 above), suggests that the effect of the ST hole on $\mathbf{P_{ST}}$ was small.

C. Comparison of measured quantities to previous studies

1. ME pressure gain

The mean $\mathbf{G_{MEP}}$ in 5 ears [including high-frequency correction, from Fig. 5(B); solid black line] ± 1 s.d. (shading) is compared to previous measurements of ME gain in chinchilla in Fig. 6. In all studies the ME was opened widely. The mean $|\mathbf{G_{MEP}}|$ in this study was about 5 dB higher than that from Ravicz *et al.* (2010), although the frequency dependence was remarkably similar, which supports the idea that the previous Ravicz *et al.* (2010) data included an uncertainty in the overall sensor sensitivity S_0 due to uncompensated temperature effects[16] (Ravicz *et al.*, 2010; see also Sec. II C 2 above).

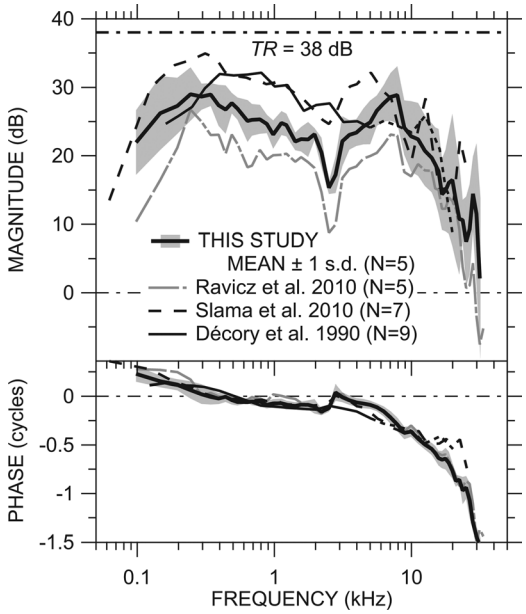

FIG. 6. Comparison of our mean $\mathbf{G_{MEP}}$ with ST intact [from Fig. 5(B); thick line] ±1 s.d. (shading) to previous measurements of ME gain in chinchilla by Ravicz *et al.* (2010, Fig. 6; sensor in ST; gray long-dashed-dotted line), Slama *et al.* (2010, Fig. 8; dashed line), and Décory *et al.* (1990, Fig. 4; thin black line solid or dotted above 5 kHz, see text) and the anatomical "transformer ratio" *TR* = 38 dB (dotted-dashed line). The ME was opened widely for all measurements. Top: Magnitude; bottom: Phase.

The mean $|\mathbf{G_{MEP}}|$ in this study is generally about 5 dB lower than the means presented by Slama *et al.* (2010, Fig. 2 and Fig. 8; dotted-dashed line) and Décory *et al.* (1990; gray line) below 5 kHz and more similar to the Décory data above 3 kHz and to the Slama data above 6 kHz. Part of the difference between our $\mathbf{G_{MEP}}$ and the ME gain of Décory *et al.* (1990) may have to do with the measurement location: In the Décory *et al.* (1990) study, sound pressure was measured in scala vestibuli (SV) at a location about 5.5 mm from the OW, which is near the best place for a 5-kHz signal. Décory *et al.* (1990) suggest that their measured SV sound pressure at higher frequencies (shown as a dotted line) might not be a good representation of SV sound pressure at the stapes.

Our mean $|\mathbf{G_{MEP}}|$ rolled off less sharply at low frequencies than ME gain in other studies, and the roll-off began at a lower frequency than in most other studies. Accordingly, our $\angle\mathbf{G_{MEP}}$ was closer to zero and crossed zero at a lower frequency than in the other studies. The Ravicz *et al.* (2010) roll-off was at a similar frequency (~250 Hz) but was much sharper. To the extent that the low-frequency roll-off seems to be related to the size of the vestibule hole and existence of cracks or other damage to the petrous bone (Slama *et al.*, 2010; Ravicz *et al.*, 2010), this result suggests that the IEs in this study were in a more intact state for the $\mathbf{G_{MEP}}$ measurements than those in the previous studies.

Our mean $|\mathbf{G_{MEP}}|$ was comparable to the other studies at high frequencies (above 8 kHz) but our $\angle\mathbf{G_{MEP}}$ accumulated much faster than that of Décory *et al.* (1990) and Slama *et al.* (2010) above 12 kHz. Our mean $|\mathbf{G_{MEP}}|$ was higher than that in the Ravicz *et al.* (2010) study above 20 kHz, which might also be a result of better experimental technique.

Figure 6 also includes the "anatomical transformer ratio" (TR) (Wever and Lawrence, 1954; Rosowski, 1994). The TR is the product of (1) the ratio of the areas of the pars tensa of the TM and the stapes footplate ("area ratio;" 56 and 2 mm^2, respectively) and (2) the ratio of the lengths of the malleus manubrium and incus long process ("lever ratio" = 2.84; all values from Vrettakos *et al.*, 1988); i.e.,

$$\mathrm{TR} = \frac{\text{TM area}}{\text{Footplate area}} \times \frac{\text{malleus length}}{\text{incus length}} = \text{area ratio} \times \text{lever ratio} \approx 79 = 38\,\text{dB}. \quad (7)$$

The mean $|\mathbf{G_{MEP}}|$ measured in this study is about 8 to 10 dB below the anatomical TR over much of the frequency range and is even further below TR near 2.5 kHz and above 10 kHz. The observation that TR overestimates $|\mathbf{G_{MEP}}|$ is consistent with observations in other species (Rosowski, 1994; Puria *et al.*, 1997) and supports the idea that the mechanical properties of the middle and IE act to limit the ear's transformer action (Wever and Lawrence, 1954; Ravicz *et al.*, 2010).

2. ST sound pressure and CP differential pressure

Our mean $\mathbf{P_{STn}}$ (of five ears from Fig. 3), adjusted by the high-frequency correction as described for $\mathbf{G_{MEP}}$ and $\mathbf{\Delta P_{CP}}$ in Sec. III D above, is compared to that from two previous studies in Fig. 7(A). Our mean $\mathbf{P_{STn}}$ is very similar to that of Ravicz *et al.* (2010) above 250 Hz and has a slightly higher magnitude at low and high frequencies than that measured in the previous study. The magnitude of the normalized $\mathbf{P_{ST}}$ from Décory *et al.* (1990) is substantially higher than our $|\mathbf{P_{STn}}|$ below 12 kHz. The phase was similar to our $\angle\mathbf{P_{STn}}$ below 12 kHz. As for $\mathbf{P_V}$ above, the Décory *et al.* (1990) data were measured at a more apical location than ours, approximately 5.5 mm from the RW; hence, we show the Décory *et al.* (1990) data with a dotted line above 5 kHz (see Sec. IV B 2 above).

Our mean $\mathbf{\Delta P_{CP}}$ [computed from five ears, from Fig. 5(C)] is compared to $\mathbf{\Delta P_{CP}}$ presented in Ravicz *et al.* (2010) and that computed from Décory *et al.* (1990, Figs. 4 and 5) in Fig. 7(B). [The Décory *et al.* (1990) data above 5 kHz are shown by a dotted line as explained above.] The differences between our $\mathbf{\Delta P_{CP}}$ and $\mathbf{\Delta P_{CP}}$ in the previous Ravicz *et al.* (2010) study are comparable to those between $\mathbf{G_{MEP}}$ in the two studies (Fig. 6). Below about 3 kHz, where $|\mathbf{P_{ST}}| \ll |\mathbf{P_V}|$, $|\mathbf{\Delta P_{CP}}|$ computed from the Décory *et al.* (1990) study[17] was 8 to 10 dB higher than ours (consistent with their $\mathbf{G_{MEP}}$; Fig. 6). (We extrapolate the computation to lower frequencies by assuming that $\mathbf{\Delta P_{CP}} \approx \mathbf{P_V}$; dotted line.) At higher frequencies, $\mathbf{\Delta P_{CP}}$ from the Décory *et al.* (1990) study was much different than ours: For example, the Décory $|\mathbf{\Delta P_{CP}}|$ decreases above 4 kHz to a dip near 8 kHz where our data increase to a $|\mathbf{\Delta P_{CP}}|$ peak, and the Décory $\angle\mathbf{\Delta P_{CP}}$ data vary in a fashion opposite to ours above 4 kHz. Our $\mathbf{\Delta P_{CP}}$ was computed in each individual ear while that for Décory *et al.* (1990) was computed from means in different ears (although there may have been some overlap), but this probably does not explain all of the difference.

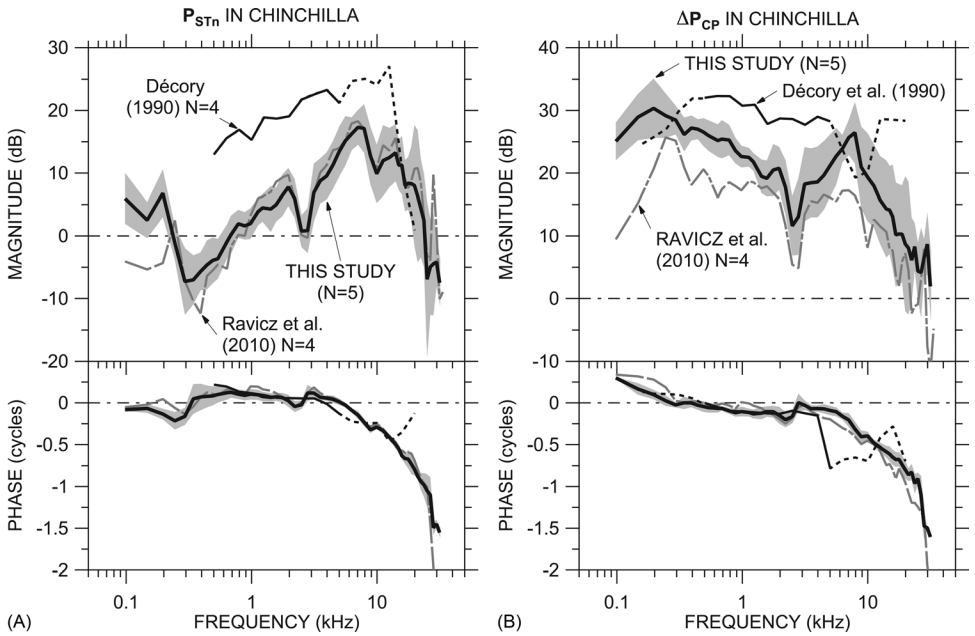

FIG. 7. Comparison of our mean $\mathbf{P_{STn}}$ and $\mathbf{\Delta P_{CP}}$ to data from previous studies. (A) Comparison of our mean $\mathbf{P_{STn}} \pm 1$ s.d. [computed from Fig. 3(A); thick line and shading] to previous measurements by Ravicz *et al.* (2010, Fig. 3; gray dotted-dashed line) and Décory *et al.* (1990, Fig. 5; thin black line solid or dotted >5 kHz, see Fig. 6). (B) Comparison of our mean $\mathbf{\Delta P_{CP}} \pm 1$ s.d. [Fig. 5(C); thick line and shading] to previous measurements by Ravicz *et al.* (2010, Fig. 8; gray dotted-dashed line) and to that computed from measurements of vestibular and ST sound pressure (not necessarily in the same ears) by Décory *et al.* [1990; thin black line solid or dotted <500 Hz (see text) and >5 kHz (see Fig. 6)]. The ME was opened widely for all measurements. Both panels: Top: Magnitude; bottom: Phase.

A comparison of Fig. 7(B) with Fig. 8 from Ravicz *et al.* (2010) shows other similarities among our $\mathbf{\Delta P_{CP}}$ and that computed for other species from other studies. As in cat, guinea pig, and gerbil, $|\mathbf{\Delta P_{CP}}|$ in chinchilla has a broad low-frequency peak and a plateau that extends to 5 kHz or beyond.

In the results we present here, the magnitude of $\mathbf{\Delta P_{CP}}$ decreases nearly to 0 dB near 28 kHz. This 0-dB-gain frequency is higher than that in previous $\mathbf{\Delta P_{CP}}$ measurements (20 kHz; Ravicz *et al.*, 2010) and is approximately equal to the high-frequency limit of chinchilla hearing (29 kHz; Rosowski, 1992). The rapid decrease of $|\mathbf{\Delta P_{CP}}|$ with frequency in this frequency range is similar to the rapid decrease in auditory sensitivity shown by the steep positive high-frequency slope to the chinchilla audiogram (e.g., Miller, 1970).

3. Ratio of ST and vestibular sound pressures

Figure 8(A) compares our mean $\mathbf{rP_{ST}}$ (from individual ears) ± s.d. to $\mathbf{rP_{ST}}$ from the previous study (Ravicz *et al.*, 2010) and that computed from the mean $\mathbf{P_{ST}}$ and $\mathbf{P_V}$ presented by Décory *et al.* (1990). The 2010 $\mathbf{rP_{ST}}$ has a similar frequency response to $\mathbf{rP_{ST}}$ from this study between 100 Hz and 25 kHz but $|\mathbf{rP_{ST}}|$ was higher in the 2010 study because $|\mathbf{G_{MEP}}|$ was lower. The minimum in $|\mathbf{rP_{ST}}|$ near 300 Hz and

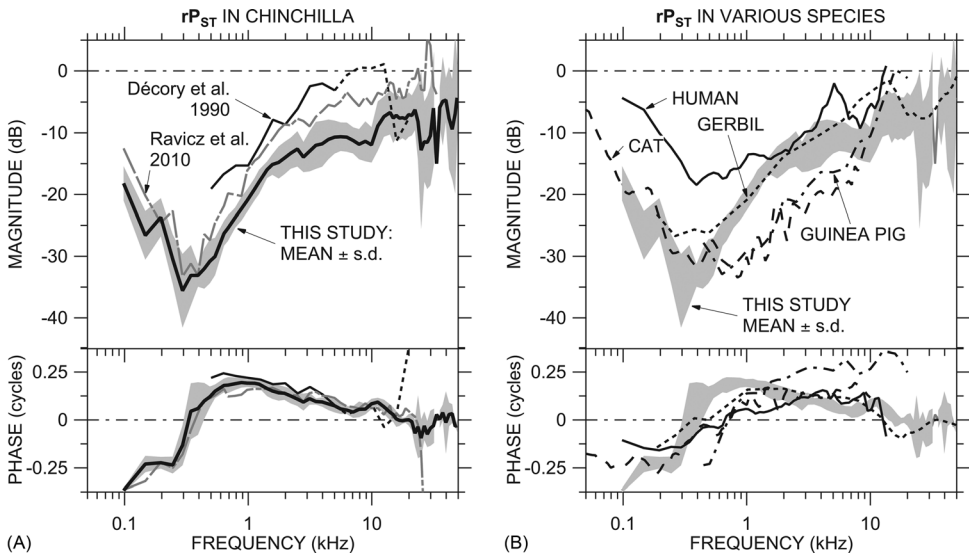

FIG. 8. Comparison of our mean $\mathbf{rP_{ST}}$ to data from previous studies. (A) Comparison of the mean $\mathbf{rP_{ST}} \pm 1$ s.d. [Fig. 3(B); thick line and shading] to $\mathbf{rP_{ST}}$ in Ravicz *et al.* (2010, Fig. 4; gray dotted-dashed line) and $\mathbf{rP_{ST}}$ computed from SV and ST sound pressures (not necessarily in the same ears) from Décory *et al.* (1990, Figs. 4 and 5; thin black line solid or dashed >5 kHz, see Sec. IV C 1). (B) Comparison of $\mathbf{rP_{ST}} \pm 1$ s.d. (shading) to that computed from SV and ST sound pressures (not necessarily in the same ears) in cat (Nedzelnitsky, 1980; dashed line), human temporal bones (Nakajima *et al.*, 2009; solid line), guinea pig (Décory *et al.*, 1990; dotted-dashed line), and gerbil (Olson, 2001; dotted line). The ME was opened widely for all measurements. Both panels: Top: Magnitude; bottom: Phase.

$\angle \mathbf{rP_{ST}} < -0.25$ cycles below 200 Hz are common to both studies.

Over the frequency range where the Décory *et al.* (1990) measurements overlap ours (0.5 to 20 kHz), $\angle \mathbf{rP_{ST}}$ was quite similar. The $|\mathbf{rP_{ST}}|$ computed from the Décory data is 10 to 15 dB higher than ours and exceeds 0 dB ($|\mathbf{P_{STn}}| > |\mathbf{G_{MEP}}|$) between 6 and 12 kHz. [The Décory *et al.* (1990) data above 5 kHz are shown by a dotted line as explained in Sec. IV C 1 above.] This difference in $\mathbf{rP_{ST}}$ between this study and Décory *et al.* (1990) will be discussed further in Sec. IV D.

The $\mathbf{rP_{ST}}$ we observed has many similar features to that computed from $\mathbf{P_{ST}}$ and $\mathbf{P_V}$ in other species [Fig. 8(B)]. $\mathbf{rP_{ST}}$ in the other species shows the low-frequency $|\mathbf{rP_{ST}}|$ minimum and $\angle \mathbf{rP_{ST}}$ transition, although the $\angle \mathbf{rP_{ST}}$ slope with frequency in the transition is less steep in most other species, implying that the resonant structures (see Sec. III B 2 above) are more highly damped in other species. $|\mathbf{rP_{ST}}|$ was generally higher in human than in chinchilla and generally lower in cat and guinea pig than in chinchilla below about 8 kHz. $\angle \mathbf{rP_{ST}}$ was higher at frequencies above 1 kHz in guinea pig than in the other species, and $|\mathbf{rP_{ST}}|$ in guinea pig also exceeded 0 dB at a high-frequency point, similar to other observations in this species (Dancer and Franke, 1980; Dancer *et al.*, 1997). $\mathbf{rP_{ST}}$ in gerbil was generally similar to $\mathbf{rP_{ST}}$ in chinchilla across the entire frequency ranges of measurements.

D. Implications of $\mathbf{rP_{ST}}$ and scalae pressures for cochlear mechanics

1. High-frequency limit on ΔP_{CP}

The ratio $\mathbf{rP_{ST}}$ contains a significant amount of information about cochlear mechanics. $\mathbf{P_{ST}}$ is the "back pressure" that reduces $\mathbf{\Delta P_{CP}}$ for a given $\mathbf{P_V}$: The more similar $|\mathbf{P_{STn}}|$ is to $|\mathbf{G_{MEP}}|$ (the closer $|\mathbf{rP_{ST}}|$ is to 0 dB), the greater the difference between $\mathbf{G_{MEP}}$ and $\mathbf{\Delta P_{CP}}$ [see Eq. (5) and Sec. III B above]. The high compliance of the RW serves to reduce $\mathbf{P_{ST}}$ at low frequencies so that most of $\mathbf{P_V}$ goes into moving the CP, although $\mathbf{P_{ST}}$ at the lowest frequencies may be due to the finite RW compliance (Nedzelnitsky, 1980). At higher frequencies, $\mathbf{P_{ST}}$ is affected by the mass of the ST perilymph between our measurement site and the RW. The high RW compliance makes $\mathbf{P_{ST}}$ just inside the RW effectively zero (e.g., Nedzelnitsky, 1980) but models of the region between the RW and the CP indicate that the mass of the ST fluid between the RW and the measurement location can explain the nonzero $\mathbf{P_{ST}}$ (Olson, 2001; Ravicz *et al.*, 2010). The value of $\mathbf{rP_{ST}}$ [−10 dB or higher; Fig. 3(B)] and the corresponding reduction in $|\mathbf{\Delta P_{CP}}|$ relative to $|\mathbf{G_{MEP}}|$ above 4 kHz [Fig. 4(B)] indicate that the mass of ST perilymph is a limitation on high-frequency $\mathbf{\Delta P_{CP}}$ and hence cochlear sensitivity.

2. Possible evidence of traveling-wave effects

We argued in Sec. IV A above that $\mathbf{P_{ST}}$ and $\mathbf{P_V}$ are due primarily to the compressional cochlear wave at most frequencies. Near 12 kHz, the presumed CF of the $\mathbf{P_{ST}}$ measurement location, $\mathbf{rP_{ST}}$ was different than at lower and higher frequencies: $|\mathbf{rP_{ST}}|$ increased abruptly to about −6 dB in all ears [see Fig. 3(B)], and $\angle \mathbf{rP_{ST}}$ reversed its downward trend with frequency and showed a broad peak at about +0.1 cycles. It is noteworthy that a similar magnitude jump is seen in $\mathbf{rP_{ST}}$ computed from the Décory *et al.* (1990) mean $\mathbf{P_{ST}}$ and $\mathbf{P_V}$ data [Fig. 8(A)] but shifted to lower frequencies: ∼5 kHz, the CF of their measurement location. As this $\mathbf{rP_{ST}}$ behavior seems to be linked to CF, it could show the influence of the traveling wave.

E. Usefulness of this preparation for studying IE function and pathology

The ability to measure sound pressures inside the cochlear scalae provides opportunities to study changes in cochlear mechanics and hearing due to pathological or unconventional methods of stimulating the cochlea, especially in preparations such as temporal bones that provide no neural response. For example: The effects of a semicircular canal dehiscence can be quantified at the level of the mechanical drive to the CP; reverse cochlear stimulation can be studied on the benchtop; and the mechanisms of stimulation of the CP by different modes of bone conduction can be compared.

The limitation on this preparation is sealing of the holes into the cochlea for the pressure sensors at low frequencies. Mathematical techniques may provide a description of the effects of the cochlear holes sufficient for a correction (Ravicz and Rosowski, 2012a), or different approaches to the cochlear vestibule (for example, through a posterior cranial fossa; Chhan *et al.*, 2012) may overcome this problem.

V. SUMMARY AND CONCLUSIONS

(1) We have measured vestibular and ST sound pressures $\mathbf{P_V}$ and $\mathbf{P_{ST}}$ with more care for calibration (Fig. 1) and measurement details than in previous studies. We have used these data and measurements of sound pressure near the TM to compute ME pressure gain $\mathbf{G_{MEP}}$ (Fig. 2), normalized ST sound pressure $\mathbf{P_{STn}}$ (Fig. 3), and the CP differential pressure at the cochlear base $\mathbf{\Delta P_{CP}}$ (Fig. 4) together in individual animals. We have used a previously-developed EC model to compute a better estimate of $\mathbf{G_{MEP}}$ and $\mathbf{\Delta P_{CP}}$ (Fig. 5) at frequencies above 15 kHz.

(2) Because $|\mathbf{P_V}| \gg |\mathbf{P_{ST}}|$ at low frequencies and $\mathbf{P_V} \approx \mathbf{P_{ST}}$ at high frequencies, $\mathbf{G_{MEP}}$ is a good estimate of $\mathbf{\Delta P_{CP}}$ at low frequencies but overestimates $\mathbf{\Delta P_{CP}}$ by a factor of 1.5 to 2 above 2 to 3 kHz (Fig. 4).

(3) $\mathbf{G_{MEP}}$ and $\mathbf{\Delta P_{CP}}$ presented here show many similarities to those presented in previous studies in chinchilla and extend those data to higher frequencies. Like other $\mathbf{G_{MEP}}$ measurements in chinchilla and other species, the magnitude of our $\mathbf{G_{MEP}}$ is smaller than the predicted anatomical *TR* (e.g. Rosowski, 1994; Puria *et al.*, 1997), with a magnitude within the range of the other studies in chinchilla (Fig. 6). $\mathbf{P_{STn}}$ presented here is very similar to

a preliminary study (Ravicz *et al.*, 2010) but our $\mathbf{P_{STn}}$ and $\mathbf{\Delta P_{CP}}$ differ substantially from results of a previous study (Décory *et al.*, 1990) in which $\mathbf{P_{ST}}$ was measured at a more apical location (Fig. 7).

(4) The ratio of $\mathbf{P_{ST}}$ to $\mathbf{P_V}$ provides insight into cochlear mechanics. Low-frequency $\mathbf{rP_{ST}}$ reveals the behavior of the RW. Near the CF of the $\mathbf{P_{ST}}$ measurement location $\mathbf{rP_{ST}}$ provides insight into how $\mathbf{rP_{ST}}$ and the differential pressure across the CP vary along the cochlea (Fig. 8).

(5) The magnitudes of both $\mathbf{G_{MEP}}$ and $\mathbf{\Delta P_{CP}}$ are shown to decrease sharply to ~0 dB as stimulus frequency increases above 20 kHz, a frequency near the high-frequency limit of audibility in chinchilla. Such behavior is consistent with a high-frequency limit to the processes that conduct sound to the IE and CP. The measured high-frequency roll-off depends on the estimate of stimulus sound pressure at the TM in the high-frequency range.

(6) Our preparation and technique is useful for several avenues of IE research at moderate and high frequencies and, with small modifications, could be more useful for low-frequency investigations as well.

ACKNOWLEDGMENTS

We thank Elizabeth Olson and Wei Dong for much help in learning to fabricate and use the pressure sensors, Elizabeth Olson for many helpful discussions, Melissa McKinnon for animal surgery and assistance with experiments, and the staff of the Eaton-Peabody Laboratory for technical support. The reviewers offered helpful comments. This work was carried out in part through the use of MIT's Microsystems Technology Laboratories and the help of Kurt Broderick and in part at the Center for Nanoscale Systems (CNS) with the help of Ed Macomber. CNS is a member of the National Nanotechnology Infrastructure Network (NNIN), which is supported by the National Science Foundation under NSF Award No. ECS-0335765, and a part of the Faculty of Arts and Sciences at Harvard University. Supported by NIDCD.

NOMENCLATURE

c	Speed of sound in water
CF	Characteristic frequency
CP	Cochlear partition
$\mathbf{c\hat{P}_{TM}}$	$\mathbf{P_{TM}}$ correction factor from an EC model
EC	Ear canal
f	Frequency (Hz)
f_0	Frequency at which pressure sensor sensitivity S_0 is evaluated
$\mathbf{G_{MEP}}$	Middle-ear pressure gain
h	Immersion depth of sensor in calibration vial
IE	Inner ear
l	Depth of water in calibration vial
ME	Middle ear
OW	Oval window
$\mathbf{P}$	Sound pressure
$\mathbf{P_{ME}}$	Sound pressure in the ME air space
$\mathbf{P_{near\text{-}TM}}$	Sound pressure measured near the TM
$\mathbf{P_{ST}}$	Sound pressure in scala tympani near the RW
$\mathbf{P_{STn}}$	Sound pressure $\mathbf{P_{ST}}$ normalized by $\mathbf{P_{TM}}$
$\mathbf{P_{TM}}$	Sound pressure at the TM
$\mathbf{P_V}$	Sound pressure in the cochlear vestibule
$\mathbf{\Delta P_{CP}}$	Sound pressure differential across the cochlear partition
$\mathbf{rP_{ST}}$	Ratio of $\mathbf{P_{ST}}$ to $\mathbf{P_V}$ with a sensor in ST
RW	Round window
s.d.	Standard deviation of the mean
$\mathbf{S_f}$	Pressure sensor frequency response
$\mathbf{S_p}$	Pressure sensor calibration as a function of f
S_0	Pressure sensor sensitivity at a given frequency f_0
ST	Scala tympani
TM	Tympanic membrane
TR	Anatomical transformer ratio
$\mathbf{v_{sens}}$	Pressure sensor output voltage
$\mathbf{\ddot{X}}$	Acceleration
ρ_w	Density of water
ω	Frequency (in radians/s) $= 2\pi f$

Real variables, e.g., S_0, are shown in italics, and complex variables, e.g., $\mathbf{P_{TM}}$, are shown in bold type. All complex variables are functions of frequency. Superscript $^{\mathbf{T}}$ refers to sound pressure measured with a sensor in scala Tympani. The circumflex (^) denotes quantities estimated from an EC model (Ravicz and Rosowski, 2012b).

[1]In this paper, real variables are shown in italics, and complex variables (e.g., $\mathbf{P_{TM}}$) with real and imaginary parts are shown in bold type.

[2]The silicon-strain-gauge hydrophones used without a probe tube by Puria and colleagues (Puria *et al.*, 1997) in SV of human temporal bones are much larger in diameter than the fiber-optic pressure sensors we use and too large to fit into the smaller cochlear scalae of chinchilla.

[3]Surgical dose: Ketamine, 40 mg/kg, administered intramuscularly and pentabarbitol (Nembutal), 50 mg/kg initial dose, administered intraperitoneally. Maintenance dose as necessary: Nembutal alternating with Ketamine at half the surgical dose. Depth of anesthesia was assessed by monitoring heart rate and toe pinch response.

[4]The frequency spacing of stimulus tones was limited at low frequencies by the 49-Hz frequency spacing of the analysis window. Chirps allowed quick overview measurements and were useful for guiding phase unwrapping of the measured sound pressures at high frequencies and checking the stability of the measurements. Tone sequences had a better signal-to-noise ratio and allowed higher stimulus levels to be used at high frequencies if necessary.

[5]The calibration accelerometer was virtually insensitive to temperature differences in the range we used (maximum −0.3 dB at 37 °C relative to 23 °C).

[6]Not all sensors were sensitive to temperature and of those that were, some showed an increase in S_0 with temperature and some showed a decrease.

[7]Calibrations on particularly sensitive sensors using many averages showed that the frequency response was smooth.

[8]We have found that during sensor insertion the sensor tip can be deflected transversely by the surface tension of perilymph seeping from the hole in the cochlea and that sometimes the sensor tip would contact the edge of the cochlear hole before entering it. In a few ears the sensitivity of one of the sensors varied by several dB throughout the experiment. By using calibrations after the sensor was withdrawn, derived scalae pressure values remained stable.

[9]The off-stimulus-frequency response was computed as the root-mean-square average of response magnitudes over a 98-Hz band (below 1 kHz; ±1 frequency point) to 294-Hz band (above 8 kHz; ±3 frequency points) about the stimulus frequency.

[10]An ossicular fixation or an increase in annular ligament stiffness or preload could also cause low $|\mathbf{G_{MEP}}|$ and stapes velocity but would not explain higher ME admittance magnitude peaks (Ravicz and Rosowski, 2012b). In contrast, damage to the stapes annular ligament or otic capsule would be expected to cause a decrease in $|\mathbf{G_{MEP}}|$ and an *increase* in

stapes velocity (see Rosowski *et al*., 2008 for a summary of the effects of ME and IE pathology on ossicular velocity and hearing in human subjects); and a reduction in RW mobility would be expected to cause a reduction in stapes velocity and an *increase* in $|\mathbf{G_{MEP}}|$.

[11]Recognizing that our small sample size makes statistical inferences difficult, we consider a mean of one population that does not overlap ± 1 s.d. of another population to indicate a statistically significant difference. For our small sample, this is roughly equivalent to the condition that the probability p that data are from the same population (the null hypothesis) is less than 5% [$p(0) < 0.05$].

[12]The model uses a pressure reflectance of 0.9 as in Ravicz and Rosowski, 2012b.

[13]Different models (e.g., Peterson and Bogert, 1950) and studies of cochlear mechanics define the fast and slow waves in different ways. We use the definition of Dong and Olson (2008) because it is clearest and has the best connection to measurable sound pressures.

[14]For example, Yoon *et al*. (2006) predict that traveling-wave pressure will be within a factor of 3 of SV pressure at 100 μm from the basilar membrane and fall off exponentially with increased distance from the membrane.

[15]Later studies have used a posterior cranial fossa approach, as mentioned in Sec. IV E below.

[16]Ravicz *et al*. (2010) noted the possibility of a temperature sensitivity of the pressure transducers but did not measure it.

[17]Note that the $\mathbf{\Delta P_{CP}}$ computed from Décory *et al*. (1990) data as presented in Ravicz *et al*. (2010) is incorrect.

Backus, J. (**1975**). "Acoustic impedance of an annular cavity," J. Acoust. Soc. Am. **58**, 1078–1081.

Beranek, L. L. (**1986**). *Acoustics* (Acoustical Society of America, Melville, NY), 491 pp.

Chhan, D., Röösli, C., McKinnon, M. L., and Rosowski, J. J. (**2012**). "Evidence of inner ear contribution in bone conduction in chinchilla," Hear. Res. (in press).

Cooper, N. P., and Rhode, W. S. (**1996**). "Fast travelling waves, slow travelling waves and their interactions in experimental studies of apical cochlear mechanics," Aud. Neurosci. **2**, 289–299.

Dallos, P. (**1970**). "Low-frequency auditory characteristics: Species dependence," J. Acoust. Soc. Am. **48**, 489–499.

Dancer, A., Avan, P., and Magnan, P. (**1997**). "Can the travelling wave be challenged by direct intracochlear pressure measurements?," in *Diversity in Auditory Mechanics*, edited by E. R. Lewis, G. R. Long, R. F. Lyon, P. M. Narins, C. R. Steele, and E. Hecht-Poinar (World Scientific, Singapore), pp. 340–346.

Dancer, A., and Franke, R. (**1980**). "Intracochlear sound pressure measurements in guinea pigs," Hear. Res. **2**, 191–205.

Décory, L., Franke, R. B., and Dancer, A. L. (**1990**). "Measurement of the middle ear transfer function in cat, chinchilla and guinea pig," in *The Mechanics and Biophysics of Hearing*, edited by P. Dallos, C. D. Geisler, J. W. Matthews, M. A. Ruggero, and C. R. Steele (Springer, Berlin), pp. 270–277.

de La Rochefoucauld, O., Decraemer, W. F., Khanna, S. M., and Olson, E. S. (**2008**). "Simultaneous measurements of ossicular velocity and intracochlear pressure leading to the cochlear input impedance in gerbil," J. Assoc. Res. Otolaryngol. **9**, 161–177.

de La Rochefoucauld, O., and Olson, E. S. (**2007**). "The role of Organ of Corti mass in passive cochlear tuning," Biophys. J. **93**, 3434–3450.

Dong, W., and Olson, E. S. (**2006**). "Middle ear forward and reverse transmission in gerbil," J. Neurophysiol. **95**, 2951–2961.

Dong, W., and Olson, E. S. (**2008**). "Supporting evidence for reverse cochlear traveling waves," J. Acoust. Soc. Am. **123**, 222–240.

Eldridge, D. H., Miller, J. D., and Bohne, B. A. (**1981**). "A frequency-position map for the chinchilla cochlea," J. Acoust. Soc. Am. **69**, 1091–1095.

Heiland, K. E., Goode, R. L., Asai, M., and Huber, A. M. (**1999**). "A human temporal bone study of stapes footplate movement," Am. J. Otol. **20**, 81–86.

Huang, G. T., Rosowski, J. J., Flandermeyer, D. T., Lynch, T. J. III, and Peake, W. T. (**1997**). "The middle ear of a lion: Comparison of structure and function to domestic cat," J. Acoust. Soc. Am. **101**, 1532–1549.

Lighthill, M. J. (**1981**). "Energy flow in the cochlea," J. Fluid Mech. **106**, 149–213.

Lupo, J. E., Koka, K., Jenkins, H. A., and Tollin, D. J. (**2012**). "Third-window vibroplasty with an active middle ear implant: Assessment of physiologic responses in a model of stapes fixation in Chinchilla lanigera," Otol. Neurotol. **33**, 425–431.

Lynch, T. J. III, Nedzelnitsky, V., and Peake, W. T. (**1982**). "Input impedance of the cochlear in cat," J. Acoust. Soc. Am. **72**, 108–130.

Merchant, S. N., and Rosowski, J. J. (**2008**). "Conductive hearing loss caused by third-window lesions of the inner ear," Otol. Neurotol. **29**, 282–289.

Miller, J. D. (**1970**). "Audibility curve of the chinchilla," J. Acoust. Soc. Am. **48**, 513–523.

Müller, M., Hoidis, S., and Smolders, J. W. T. (**2010**). "A physiological frequency-position map of the chinchilla cochlea," Hear. Res. **268**, 184–193.

Nakajima, H. H., Dong, W., Olson, E. S., Merchant, S. N., Ravicz, M. E., and Rosowski, J. J. (**2009**). "Differential intracochlear sound pressure measurements in normal human temporal bones," J. Assoc. Res. Otolaryngol. **10**, 23–36.

Nedzelnitsky, V. (**1980**). "Sound pressure in the basal turn of the cat cochlea," J. Acoust. Soc. Am. **68**, 1676–1689.

Olson, E. S. (**1998**). "Observing middle and inner ear mechanics with novel intracochlear pressure sensors," J. Acoust. Soc. Am. **103**, 3445–3463.

Olson, E. S. (**2001**). "Intracochlear pressure measurements related to cochlear tuning," J. Acoust. Soc. Am. **110**, 349–367.

Peake, W. T., Rosowski, J. J., and Lynch, T. J., III. (**1992**). "Middle-ear transmission: Acoustic versus ossicular coupling in cat and human," Hear. Res. **57**, 245–268.

Peterson, L. C., and Bogert, B. P. (**1950**). "A dynamical theory of the cochlea," J. Acoust. Soc. Am. **22**, 369–381.

Puria, S., and Allen, J. B. (**1991**). "A parametric study of cochlear input impedance," J. Acoust. Soc. Am. **89**, 287–309; **89**, 2463(E) (1991).

Puria, S., Peake, W. T., and Rosowski, J. J. (**1997**). "Sound-pressure measurements in the cochlear vestibule of human-cadaver ears," J. Acoust. Soc. Am. **101**, 2754–2770.

Ravicz, M. E., Chhan, D. C., and Rosowski, J. J. (**2011**). "Efficiency of chinchilla middle ears," in *Abstracts of the 34th Midwinter Meeting of the Association for Research in Otolaryngology* (Association for Research in Otolaryngology, Mt. Royal, NJ), #47 (abstract).

Ravicz, M. E., Olson, E. S., and Rosowski, J. J. (**2007**). "Sound pressure distribution and power flow within the gerbil ear canal from 100 Hz to 80 kHz," J. Acoust. Soc. Am. **122**, 2154–2163.

Ravicz, M. E., and Rosowski, J. J. (**2012a**). "A new estimate of the middle-ear transmission matrix in chinchilla," in *Abstracts of the 35th Midwinter Meeting of the Association for Research in Otolaryngology* (Association for Research in Otolaryngology, Mt. Royal, NJ), #126 (abstract).

Ravicz, M. E., and Rosowski, J. J. (**2012b**). "Chinchilla middle-ear admittance and sound power: High-frequency estimates and effects of inner-ear modifications." J. Acoust. Soc. Am. **132**, 2437–2454.

Ravicz, M. E., Rosowski, J. J., and Voigt, H. F. (**1992**). "Sound-power collection by the auditory periphery of the Mongolian gerbil Meriones unguiculatus: I. Middle-ear input impedance," J. Acoust. Soc. Am. **92**, 157–177.

Ravicz, M. E., Slama, M. C. C., and Rosowski, J. J. (**2010**). "Middle-ear pressure gain and cochlear partition differential pressure in chinchilla," Hear Res. **263**, 16–25.

Rosowski, J. J. (**1992**). "Hearing in transitional mammals: Predictions from the middle-ear anatomy and hearing capabilities of extant mammals," in *The Evolutionary Biology of Hearing*, edited by D. B. Webster, A. N. Popper, and R. R. Fay (Springer-Verlag, New York), pp. 615–631.

Rosowski, J. J. (**1994**). "Outer and middle ear," in *Comparative Hearing in Mammals*, edited by A. N. Popper and R. R. Fay (Springer-Verlag, New York), pp. 173–247.

Rosowski, J. J., Nakajima, H. H., and Merchant, S. N. (**2008**). "Clinical utility of laser-Doppler vibrometer measurements in live normal and pathologic human ears," Ear Hear. **29**, 3–19.

Rosowski, J. J., Ravicz, M. E., and Songer, J. E. (**2006**). "Structures that contribute to middle-ear admittance in chinchilla," J. Comp. Physiol., A. **192**, 1287–1311.

Ruggero, M. A., Rich, N. C., Robles, L., and Shivapuja, B. G. (**1990**). "Middle-ear response in the chinchilla and its relationship to mechanics at the base of the cochlea," J. Acoust. Soc. Am. **87**, 1612–1629.

Schloss, F., and Strasberg, M. (**1962**). "Hydrophone calibration in a vibrating column of liquid," J. Acoust. Soc. Am. **34**, 958–960.

Shera, C. A., and Zweig, G. (**1992**). "Middle-ear phenomenology: The view from the three windows," J. Acoust. Soc. Am. **92**, 1356–1370.

Slama, M. C. C., Ravicz, M. E., and Rosowski, J. J. (**2010**). "Middle ear function and cochlear input impedance in chinchilla," J. Acoust. Soc. Am. **127**, 1397–1410.

Songer, J. E., and Rosowski, J. J. (**2006**). "The effect of superior-canal opening on middle ear input admittance and air-conducted stapes velocity in chinchilla." J. Acoust. Soc. Am. **120**, 258–269.
von Békésy, G. (**1947**). "The sound pressure difference between the round and the oval windows and the artificial window of labyrinthine fenestration," Acta Oto-Laryngol. **35**, 301–315. In von Békésy, G. (**1960**). *Experiments in Hearing* (McGraw-Hill, New York), pp. 115–126.
Voss, S. E., Rosowski, J. J., and Peake, W. T. (**1996**). "Is the pressure difference between the oval and round windows the effective acoustic stimulus for the cochlea?," J. Acoust. Soc. Am. **100**, 1602–1616.
Vrettakos, P. A., Dear, S. P., and Saunders, J. C. (**1988**). "Middle ear structure in the chinchilla: A quantitative study," Am. J. Otolaryngol. **9**, 58–67.
Wever, E. G., and Lawrence, M. (**1954**). *Physiological Acoustics* (Princeton University Press, Princeton, NJ), 454 pp.
Yoon, Y.-J., Puria, S., and Steele, C. R. (**2006**). "Intracochlear pressure and organ of Corti impedance from a linear active three-dimensional model," ORL **68**, 365–372.
Zwislocki, J. J. (**1962**). "Analysis of the middle-ear function. Part I: Input impedance," J. Acoust. Soc. Am. **34**, 1514–1523.